Light top squarks in a $U(1)_R$ lepton number model with a right handed neutrino and the LHC

Sabyasachi Chakraborty,[1,*] AseshKrishna Datta,[2,†] Katri Huitu,[3,‡] Sourov Roy,[1,§] and Harri Waltari[3,‖]

[1]*Department of Theoretical Physics, Indian Association for the Cultivation of Science, 2A & 2B Raja S. C. Mullick Road, Jadavpur, Kolkata 700 032, India*

[2]*Harish-Chandra Research Institute, Chhatnag Road, Jhunsi, Allahabad 211019, India*

[3]*Department of Physics and Helsinki Institute of Physics, University of Helsinki, P. O. Box 64, Helsinki FIN-00014, Finland*

(Received 4 September 2015; published 5 April 2016)

We investigate the phenomenology of top squarks at the Large Hadron Collider (LHC) in a supersymmetric model where lepton number is identified with an approximate $U(1)_R$ symmetry in such a way that one of the left-chiral sneutrinos can acquire a large vacuum expectation value and can play the role of the down-type Higgs. This R symmetry allows a subset of trilinear R-parity violating interactions, which determine the collider phenomenology of this model in a significant way. The gauginos are Dirac particles and gluinos are relatively heavy in this class of models. The model contains a right handed neutrino superfield, which gives a tree level mass to one of the active neutrinos. An order one neutrino Yukawa coupling also helps enhance the Higgs boson mass at the tree level and results in a very light bino-like neutralino ($\tilde{\chi}_2^0$) with mass around a few hundred MeV, which is a carrier of missing (transverse) energy ($\not{E}_T$). The model can accommodate two rather light top squarks, compatible with the observed mass of the Higgs boson. The lighter top squark ($\tilde{t}_1$) can decay into $t\tilde{\chi}_2^0$, and thus the signal would be similar to the signal of top quark pair production at the LHC. In addition, fully visible decays such as $\tilde{t}_2 \to be^+$ can give rise to interesting final states. Such signals at the LHC combined with other features like a heavy gluino could provide strong evidence for this kind of a model. Our analysis shows that $m_{\tilde{t}_1} \lesssim 575(750)$ GeV and $m_{\tilde{t}_2} \lesssim 1.2(1.4)$ TeV can be probed with 5σ statistical significance at the 13 TeV LHC with $300(3000)$ fb^{-1} of integrated luminosity. Finally, we observe that in the presence of superlight carriers of $\not{E}_T$, the so-called "stealth" top squark scenario may naturally appear in our model.

DOI: 10.1103/PhysRevD.93.075005

I. INTRODUCTION

The discovery of a Higgs boson at the Large Hadron Collider (LHC) with a mass around 125 GeV [1,2] is of immense importance in high energy physics and, in particular, in the context of electroweak symmetry breaking. However, in spite of its enormous success over the years, the Standard Model (SM) of particle physics suffers from several drawbacks. From a theoretical perspective, the naturalness problem remains a troublesome issue in the framework of SM. Supersymmetry (SUSY) renders an elegant solution to this problem and has become the most popular choice for physics beyond the Standard Model to date. Nevertheless, searches for superpartners by the LHC collaborations (ATLAS and CMS) in pp collisions at the center-of-mass energies of $\sqrt{s} = 7$ and 8 TeV have shown no significant excess [3,4] over the SM background. This has put stringent lower limits on the superpartner masses in many different SUSY scenarios. Recent experimental analyses within the framework of a simplified phenomenological minimal supersymmetric Standard Model have set a lower bound of 1.7 TeV [5] for comparable masses of the gluino and the first two generation squarks.

On top of that, finding a Higgs boson with a mass ~125 GeV and the nonobservation of any signals of physics beyond the SM have severely constrained many supersymmetric scenarios which are otherwise very well motivated. In view of this, models with Dirac gauginos and $U(1)_R$ symmetry have become popular as they can significantly lower the current exclusion bounds on the first and second generation squarks and at the same time can address the 125 GeV Higgs boson even in the presence of lighter top squarks. Other virtues of such scenarios include significant suppression of flavor- as well as CP-violating effects. Assorted versions of models with Dirac gauginos and $U(1)_R$ symmetry can be found in the literature [6–67].

On the other hand, experiments in the neutrino sector have firmly established the fact that neutrinos have tiny masses and nontrivial mixings. Nonvanishing neutrino masses and mixings [68–71] are very important indications of new physics. An interesting question to investigate is

*tpsc3@iacs.res.in
†asesh@hri.res.in
‡katri.huitu@helsinki.fi
§tpsr@iacs.res.in
‖harri.waltari@helsinki.fi

whether models with Dirac gauginos could also provide explanation for observed neutrino masses and mixings. As we shall describe later on, the introduction of a right handed neutrino superfield with an appropriate R charge and Yukawa coupling "f" can give rise to a small neutrino mass of the right order at the tree level. At the same time, an order one f generates an additional tree level contribution to the Higgs boson mass. Thus, physics in the Higgs sector and the physics in the neutrino sector become intimately related in this model. This gives an opportunity to look into the Higgs sector through the neutrino window and vice versa. The additional tree level contribution to the Higgs boson mass also opens up the possibility of having rather light top squarks in the spectrum. This can also ameliorate the situation with so-called "naturalness" that is somewhat compromised in popular SUSY frameworks like the minimal supersymmetric Standard Model (MSSM). There, the top squark masses are pushed to higher values [$\sim\mathcal{O}$(TeV)] to ensure a Higgs boson as heavy as observed at the LHC. Another very interesting outcome of this scenario is to have a very light bino-like neutralino, also identified as the lightest supersymmetric particle (LSP), with a mass in the range of a few hundred MeV. The scenario violates R parity. Thus, such a light neutralino LSP could decay to SM fermions. However, the decay length turns out to be much larger than the collider dimension [72]. Hence it would essentially contribute to missing transverse energy (MET; $\not{E}_T$).

In such a backdrop, we study the phenomenology of light top squarks at the LHC in a $U(1)_R$ symmetric model, first introduced in Refs. [45,46] and later on augmented by a right handed neutrino superfield in Refs. [52,58,63]. The R charges are identified with the lepton numbers in such a way that the left-chiral sneutrino vacuum expectation values (VEVs) can be large, and are not constrained by the Majorana mass of the neutrinos. Thus, the sneutrino can play the role of a down-type Higgs field. There also exists a subset of R-parity violating (RPV) operators, mixings between the neutrinos and the neutralinos, as well as between the charged leptons and the charginos. Once $U(1)_R$ symmetry is invoked, the gauginos cease to have Majorana masses. However, they can acquire Dirac masses which requires additional chiral superfields living in the adjoint representation of the SM gauge group. It is somewhat crucial in the context of the present work to note that R-symmetric models also prohibit the traditional trilinear scalar couplings ("A" terms) and the Higgsino mass parameter (μ term). To generate a μ term, one needs to incorporate two more chiral superfields R_u and R_d with appropriate R charges.

The main motivation for having a right handed neutrino superfield is to have a tree level neutrino mass [52]. However, such a simple extension has enormous implication for the lightest CP-even Higgs boson mass [52,63] and for the dark matter sector [58].

The squarks in the present context carry a nonzero R charge ($R = 1$) and hence a nonzero lepton number since lepton number is identified with the R charges. Top squarks can naturally be light in this model and can have novel signatures at the LHC. In the present work, we take the obviously natural direction of connecting to the top squark sector which is very much in the focus of the current LHC program and thus could be put to test in a straightforward way. This work presents for the first time the collider implications of the very characteristic top squark sector of the scenario under consideration. Various possibilities in the decays of both top squarks are discussed in detail. A novel final state in the form of $b\bar{b}e^+e^-$ is highlighted where the final state objects can, in principle, be reconstructed to the mass of the heavier top squark. The decay of the top squark to be^+ differs from typical R-parity violating MSSM decay modes, and is typical for this model. This also provides us with an interesting handle, using which the reach of $\tilde{t}_2$ can be enhanced significantly, so much so, that the enhanced rate could also lead to its discovery even before its lighter cousin.

As for $\tilde{t}_1$, pair production of top squarks and their subsequent decays might lead to a signal similar to top quark pair production and provide important information on the model and, in particular, on the scenario with an order one neutrino Yukawa coupling f. A characteristic difference in the signal is in the form of a somewhat softer $\not{E}_T$, when compared to similar $m_{\tilde{t}_1}$ values in the MSSM. This is because of the presence of a MeV neutralino LSP, which is again a salient feature of our scenario. It is also demonstrated how various decay modes of $\tilde{t}_1$ remain simultaneously open thus necessitating a thorough analysis of the experimental data from the 13 TeV run of the LHC.

The paper is organized as follows. A brief description of the model is presented in Sec. II. The neutral scalar sector of the model and its characteristic features are discussed in Sec. III. Section IV describes the electroweak gauginos in general. We start with a generic discussion of the neutralino sector and its role in generating the tree level neutrino mass both in $U(1)_R$ conserving case as well as taking into account mild violation of this R symmetry. We discuss the possibility of mixings among the neutralinos and the neutrinos. Later on, we discuss the chargino sector of this model and the corresponding mixing between the charginos and the electron. The focus area of this work, that is to say, the top squark sector is described in Sec. V. Expressions for the decay rates in various relevant modes are presented. The latest bounds on the masses of the top squarks as reported by the LHC collaborations are also discussed. The model is incorporated in SARAH (v4.4.1) [73–75]. In Sec. VI we present a few benchmark points that reflect the characteristic decay patterns of the two top squarks and are found to be instrumental in shaping the interesting signatures at the LHC. Section VII is devoted to the actual simulation study of the signals and the most relevant backgrounds using event generators. Estimations of the reaches in the masses of the top squarks are also presented. In Sec. VIII we briefly analyze the issue of the stealth top squark which arises

naturally in our scenario. We summarize with some concluding remarks in Sec. IX.

II. THE $U(1)_R$ LEPTON NUMBER MODEL

We minimally extend an R-symmetric model, first discussed in [45,46], by a single right handed neutrino superfield $\hat{N}^c$ [52]. Along with the chiral superfields of the MSSM superfields, $\hat{H}_u$, $\hat{H}_d$, $\hat{Q}_i$, $\hat{U}_i^c$, $\hat{D}_i^c$, $\hat{L}_i$, $\hat{E}_i^c$, the model contains two "inert" doublet superfields $\hat{R}_u$ and $\hat{R}_d$ with opposite hypercharges. To prohibit spontaneous R breaking and hence the emergence of R axions, the scalar components of $\hat{R}_u$ and $\hat{R}_d$ are barred from receiving any nonzero VEV. This is why $\hat{R}_u$ and $\hat{R}_d$ are labeled as inert. Similarly, the scalar component of $\hat{N}^c$ does not acquire any nonzero VEV. The Dirac gaugino masses can be constructed with the introduction of chiral superfields living in the adjoint representation of the SM gauge group. A singlet $\hat{S}$ is needed to form a Dirac mass for the $U(1)$ gaugino, a triplet $\hat{T}$ under $SU(2)_L$ is required to have a Dirac mass for the $SU(2)_L$ gauginos and similarly an octet $\hat{O}$ under $SU(3)_C$ must be there to generate the Dirac gluino mass. The $U(1)_R$ charges of the chiral superfields along with their SM gauge quantum numbers are shown in Table I.

Note that the scalar components transform in the same manner as their respective chiral superfields whereas the fermions have R charge one less than that of the corresponding chiral superfields. Following Ref. [45], we also identify the lepton numbers of the component fields to the negative of their R charges. Such an identification leaves the lepton number assignments of the SM fermions unchanged from the usual ones while the superpartners acquire nonstandard lepton numbers. As mentioned in the Introduction, it is quite conspicuous that the left-chiral sneutrino VEVs can be large since they do not become constrained by the lepton-number-violating Majorana neutrino masses [45]. As a result, the sneutrino can play the role of a down-type Higgs field. It is now possible to integrate out the superfields $\hat{R}_u$ and $\hat{H}_d$, which simplifies the superpotential and the scalar potential considerably. At this point all three sneutrinos can acquire substantial VEVs. However, without any loss of generality, one can always choose a basis in which only one of the sneutrinos get a nonzero VEV, which we choose to be the electron-type sneutrino,[1] whereas, the VEVs of the other two sneutrino fields are zero. Thus, the electron sneutrino ($[\tilde{\nu}_a, a = 1(e)]$ plays the role of a down-type Higgs field. With this basis choice and the assumptions of [52,63], the superpotential takes the following form:

[1]It should be noted at this point that the formulation, though independent of this kind of a choice of a particular basis, could have crucial impacts on the actual observables at the experiments. We justify our choice later in this paragraph.

TABLE I. Chiral superfields with the SM gauge quantum numbers and $U(1)_R$ charge assignments.

Superfields	$SU(3)_C$, $SU(2)_L$, $U(1)_Y$	$U(1)_R$
$\hat{Q}$	$(3, 2, \frac{1}{3})$	1
$\hat{U}_i^c$	$(\bar{3}, 1, -\frac{4}{3})$	1
$\hat{D}_i^c$	$(\bar{3}, 1, \frac{2}{3})$	1
$\hat{L}_i$	$(1, 2, -1)$	0
$\hat{E}_i^c$	$(1, 1, 2)$	2
$\hat{H}_u$	$(1, 2, 1)$	0
$\hat{H}_d$	$(1, 2, -1)$	0
$\hat{R}_u$	$(1, 2, 1)$	2
$\hat{R}_d$	$(1, 2, -1)$	2
$\hat{S}$	$(1, 1, 0)$	0
$\hat{T}$	$(1, 3, 0)$	0
$\hat{O}$	$(8, 1, 0)$	0
$\hat{N}^c$	$(1, 1, 0)$	2

$$W = y_{ij}^u \hat{H}_u \hat{Q}_i \hat{U}_j^c + \mu_u \hat{H}_u \hat{R}_d + f \hat{L}_a \hat{H}_u \hat{N}^c + \lambda_S \hat{S} \hat{H}_u \hat{R}_d + 2\lambda_T \hat{H}_u \hat{T} \hat{R}_d - M_R \hat{N}^c \hat{S} + W', \quad (1)$$

$$W' = \sum_{b=2,3} f_b^l \hat{L}_a \hat{L}'_b \hat{E}_b'^c + \sum_{k=1,2,3} f_k^d \hat{L}_a \hat{Q}'_k \hat{D}_k'^c + \sum_{k=1,2,3} \frac{1}{2} \tilde{\lambda}_{23k} \hat{L}'_2 \hat{L}'_3 \hat{E}_k'^c + \sum_{j,k=1,2,3;b=2,3} \tilde{\lambda}'_{bjk} \hat{L}'_b \hat{Q}'_j \hat{D}_k'^c, \quad (2)$$

where y_{ij}^u is the up-type Yukawa coupling, μ_u is the Higgsino mass parameter consistent with the R-charge assignments. f represents the neutrino Yukawa coupling, λ_S and λ_T are the trilinear couplings and finally M_R is the coefficient of the bilinear term $\hat{N}^c \hat{S}$.

Note that for simplicity in this work we have neglected the terms $\kappa \hat{N}^c \hat{S} \hat{S}$, $\eta \hat{N}^c$, $\xi \hat{N}^c \mathrm{Tr}(\hat{T} \hat{T})$ and $\zeta \hat{N}^c \mathrm{Tr}(\hat{O} \hat{O})$ from the superpotential. As long as $\eta \sim M_{\mathrm{SUSY}}^2$, κ, ξ, $\zeta \sim 1$ and VEVs of the scalar components of $\hat{S}$ and $\hat{T}$ are very small [$\sim \mathcal{O}(10^{-4})$ GeV, as we shall consider later], we do not expect any significant changes in the analysis and the results presented in this work.

The prime in W' indicates the mass basis for the down-type quarks and charged leptons. When the electron sneutrino gets a VEV, the first two terms in W' give masses to the down-type charged leptons and quarks. However, $SU(2)$ invariance ensures that LLE operator in Eq. (2) cannot generate a mass for the electron. The electron mass can be generated from higher-dimensional operators suppressed by a mass scale as discussed in [45]. Such operators would, in principle, contribute to the masses of other charged leptons as well. However, these contributions will be subdominant compared to the contribution to their masses from the LLE operators. This makes it a natural choice for the electron sneutrino to acquire a

nonzero VEV. The other two terms in W' include all the trilinear R-parity violating but *lepton number preserving* terms in this model.

In a realistic supersymmetric model, one needs to incorporate soft-SUSY breaking terms such as the gaugino and the scalar mass terms. The Lagrangian consisting of the Dirac gaugino mass terms [45] can be written as

$$\mathcal{L}^{\rm Dirac}_{\rm gaugino} = \int d^2\theta \frac{W'_\alpha}{\Lambda}[\sqrt{2}\kappa_1 W_{1\alpha}\hat{S} + 2\sqrt{2}\kappa_2 {\rm tr}(W_{2\alpha}\hat{T}) + 2\sqrt{2}\kappa_3 {\rm tr}(W_{3\alpha}\hat{O})] + {\rm H.c.}, \quad (3)$$

where $W'_\alpha = \lambda_\alpha + \theta_\alpha D'$ is a spurion superfield parametrizing D-type SUSY breaking. $W_{i\alpha}$'s are the field strength tensors containing the gauginos of the MSSM vector superfields. The D-term VEV generates Dirac gaugino masses which can be schematically written as $M_i^D = \kappa_i \frac{\langle D' \rangle}{\Lambda}$, where κ_i's are the order one coefficients and Λ is the scale of SUSY mediation.

Similarly, R-conserving but soft-SUSY breaking terms in the scalar sector can be generated from a spurion superfield $\hat{X}$, where $\hat{X} = x + \theta^2 F_X$ [45]. The nonzero VEV of the F term generates the scalar soft terms. In the rotated basis where only the electron-type sneutrino acquires a VEV, the soft-SUSY breaking terms are given by

$$\begin{aligned} V_{\rm soft} &= m^2_{H_u} H_u^\dagger H_u + m^2_{R_d} R_d^\dagger R_d + m^2_{\tilde{L}_a} \tilde{L}_a^\dagger \tilde{L}_a + \sum_{b=2,3} m^2_{\tilde{L}_b} \tilde{L}_b^\dagger \tilde{L}_b + M_N^2 \tilde{N}^{c\dagger} \tilde{N}^c + m^2_{\tilde{R}_i} \tilde{l}^\dagger_{Ri} \tilde{l}_{Ri} + m^2_{\tilde{Q}_i} \tilde{Q}_i^\dagger \tilde{Q}_i + m^2_{\tilde{u}_i} \tilde{u}^\dagger_{Ri} \tilde{u}_{Ri} \\ &+ m^2_{\tilde{d}_i} \tilde{d}^\dagger_{Ri} \tilde{d}_{Ri} + m_S^2 S^\dagger S + 2m_T^2 {\rm tr}(T^\dagger T) + 2m_O^2 {\rm tr}(O^\dagger O) - (B\mu_L H_u \tilde{L}_a + {\rm H.c.}) + (t_S S + {\rm H.c.}) \\ &+ \frac{1}{2} b_S (S^2 + {\rm H.c.}) + b_T ({\rm tr}(TT) + {\rm H.c.}) + B_O ({\rm tr}(OO) + {\rm H.c.}). \end{aligned} \quad (4)$$

It is important to note that the scalar singlet tadpole term ($t_S S$) is suppressed [42] in the scenarios with Dirac gaugino masses and that is what we will consider in the present context. With this short description of the theoretical framework we now proceed to describe the scalar and the fermionic sectors of the model in appropriate details.

III. THE NEUTRAL SCALAR SECTOR AND THE STANDARD-MODEL-LIKE HIGGS BOSON

In this section we discuss the CP-even scalar sector followed by a rather important discussion on the lightest CP-even mass eigenstate. The scalar potential receives contributions from the F term, the D term, the soft-SUSY breaking terms and the dominant quartic terms generated at one loop and can be written down as

$$V = V_F + V_D + V_{\rm soft} + V_{\text{one-loop}}. \quad (5)$$

From the scalar potential and the subsequent minimization equations, one can now write down the CP-even scalar mass matrix in the basis $(h_R, \tilde{\nu}_R, S_R, T_R)$, where the subscript R indicates the real parts of the corresponding superfields. Both R_d and $\tilde{N}^c$ carry R charges of two units and hence get decoupled from the CP-even scalar mass matrix. In the R-symmetric scenario the elements of CP-even 4×4 scalar mass matrix are given by [52]

$$\begin{aligned} (M_S^2)_{11} &= \frac{(g^2+g'^2)}{2} v^2 \sin^2\beta + (f M_R v_S - B\mu_L^a)(\tan\beta)^{-1} + 2\delta\lambda_u v^2 \sin^2\beta, \\ (M_S^2)_{12} &= f^2 v^2 \sin 2\beta + B\mu_L^a - \frac{(g^2+g'^2-2\delta\lambda_3)}{4} v^2 \sin 2\beta - f M_R v_S, \\ (M_S^2)_{13} &= 2\lambda_S^2 v_S v \sin\beta + 2\mu_u \lambda_S v \sin\beta + 2\lambda_S \lambda_T v v_T \sin\beta + \sqrt{2} g' M_1^D v \sin\beta - f M_R v \cos\beta, \\ (M_S^2)_{14} &= 2\lambda_T^2 v_T v \sin\beta + 2\mu_u \lambda_T v \sin\beta + 2\lambda_S \lambda_T v_S v \sin\beta - \sqrt{2} g M_2^D v \sin\beta, \\ (M_S^2)_{22} &= \frac{(g^2+g'^2)}{2} v^2 \cos^2\beta + (f M_R v_S - B\mu_L^a)\tan\beta + 2\delta\lambda_\nu v^2 \cos^2\beta, \\ (M_S^2)_{23} &= -\sqrt{2} g' M_1^D v \cos\beta - f M_R v \sin\beta, \\ (M_S^2)_{24} &= \sqrt{2} g M_2^D v \cos\beta, \\ (M_S^2)_{33} &= -\mu_u \lambda_S \frac{v^2 \sin^2\beta}{v_S} - \frac{\lambda_S \lambda_T v_T v^2 \sin^2\beta}{v_S} - \frac{t_S}{v_S} + \frac{g' M_1^D v^2 \cos 2\beta}{\sqrt{2} v_S} + \frac{f M_R v^2 \sin 2\beta}{2 v_S}, \\ (M_S^2)_{34} &= \lambda_S \lambda_T v^2 \sin^2\beta, \\ (M_S^2)_{44} &= -\mu_u \lambda_T \frac{v^2}{v_T} \sin^2\beta - \lambda_S \lambda_T v_S \frac{v^2}{v_T} \sin^2\beta - \frac{g M_2^D}{\sqrt{2}} \frac{v^2}{v_T} \cos 2\beta. \end{aligned} \quad (6)$$

The δ's appearing only in $(M_S^2)_{11}$, $(M_S^2)_{12}$ and $(M_S^2)_{22}$ quantify the dominant one-loop radiative corrections[2] to the quartic potential coming from the terms $\frac{1}{2}\delta\lambda_u(|H_u|^2)^2$, $\frac{1}{2}\delta\lambda_3|H_u^0|^2|\tilde{\nu}_a|^2$ and $\frac{1}{2}\delta\lambda_\nu(|\tilde{\nu}_a|^2)^2$ where

$$\begin{aligned}
\delta\lambda_u &= \frac{3y_t^4}{16\pi^2}\ln\left(\frac{m_{\tilde{t}_1}m_{\tilde{t}_2}}{m_t^2}\right)+\frac{5\lambda_T^4}{16\pi^2}\ln\left(\frac{m_T^2}{v^2}\right)+\frac{\lambda_S^4}{16\pi^2}\ln\left(\frac{m_S^2}{v^2}\right)+\cdots,\\
\delta\lambda_3 &= \frac{5\lambda_T^4}{32\pi^2}\ln\left(\frac{m_T^2}{v^2}\right)+\frac{\lambda_S^2}{32\pi^2}\ln\left(\frac{m_S^2}{v^2}\right)+\cdots,\\
\delta\lambda_\nu &= \frac{3y_b^4}{16\pi^2}\ln\left(\frac{m_{\tilde{b}_1}m_{\tilde{b}_2}}{m_t^2}\right)+\frac{5\lambda_T^4}{16\pi^2}\ln\left(\frac{m_T^2}{v^2}\right)+\frac{\lambda_S^4}{16\pi^2}\ln\left(\frac{m_S^2}{v^2}\right)+\cdots
\end{aligned} \tag{7}$$

m_S, m_T are the singlet and triplet soft masses while the singlet and the triplet VEVs are denoted by v_S and v_T, respectively [22]. g', g are the $U(1)_Y$ and $SU(2)_L$ gauge coupling constants, M_1^D, M_2^D are the Dirac bino and wino masses, respectively. $\tan\beta = v_u/v_a$, where v_u is the VEV of the up-type neutral Higgs field and v_a represents the VEV of the electron-type sneutrino. The ellipsis at the end of each expression stands for missing subdominant terms.

In this work, we study a simplified scenario in which the singlet and the triplet VEVs are very small. These effectively decouple the corresponding scalar fields. Thus, the CP-even scalar mass-squared matrix turns out to be a 2×2 one and can be written down in a compact form as

$$\begin{aligned}
M_{11}^2 &= M_Z^2\sin^2\beta+\xi\cot\beta,\\
M_{12}^2 &= -\xi+\frac{1}{2}M_Z^2(\alpha-1)\sin 2\beta = M_{21}^2,\\
M_{22}^2 &= \xi\tan\beta+M_Z^2\cos^2\beta,
\end{aligned} \tag{8}$$

where $\alpha=\frac{2f^2v^2}{M_Z^2}$ and $\xi = fM_Rv_S - B\mu_L$. As long as $M_A^2 > M_Z^2$, where $M_A^2 \equiv \frac{2(-B\mu_L+fM_Rv_S)}{\sin 2\beta}$ is the CP-odd Higgs mass, we find that the tree level upper bound on the lightest CP-even Higgs boson mass is [52]

$$m_h^2 \le [M_Z^2\cos^2 2\beta + f^2v^2\sin^2 2\beta]. \tag{9}$$

Clearly, this result is very interesting since for a large neutrino Yukawa coupling, $f\sim\mathcal{O}(1)$, the Higgs boson mass receives a large tree level enhancement. This additional tree level contribution $(\Delta m_h^2)_{\rm Tree} = f^2v^2\sin^2 2\beta$ grows at low $\tan\beta$ and becomes significant for order one neutrino Yukawa coupling f [52,63]. The resulting enhancement could play a significant role in lifting the Higgs boson mass to 125 GeV. Furthermore, this additional contribution ameliorates the naturalness (pertaining to the mass of the Higgs boson) issue in the MSSM. However, this tree level contribution gets diluted at large values of $\tan\beta$. There, the one-loop quartic corrections [22,45] can come into play and can substantially enhance the Higgs boson mass in the presence of order one couplings, λ_S and λ_T, as shown in Eq. (7). Thus, even for larger values of $\tan\beta$, one can easily find a Higgs boson as heavy as observed at the LHC experiments, when the top squarks are relatively light. Figure 1 illustrates the region in the plane of $m_{\tilde{t}_1}$ and $m_{\tilde{t}_2}$ compatible with 124.7 GeV $< m_h <$ 126.2 GeV and various slices of λ_S over the ranges shown. This takes into account the one-loop corrections computed in the effective potential approach to the neutral scalar potential as implemented in SARAH (v4.4.1) [73–75]. For this scattered plot we use $\tan\beta = 23$, $M_1^D = M_2^D = 1.2$ TeV, $M_3^D = 1.5$ TeV, $\mu_u = 200$ GeV, $f = 1$, $v_S = v_T = 10^{-4}$ GeV, $B\mu_L = -(200\ \text{GeV})^2$, $t_S = (174\ \text{GeV})^3$ and vary λ_S in the range $0.8 < \lambda_S \le 1.3$. We also vary the soft scalar masses $(m_Q^2)_{33}$, $(m_u^2)_{33}$ in the range $-8\times 10^6\ (\text{GeV})^2$ to $8\times 10^6\ (\text{GeV})^2$ to vary the top squark mass. We observe that higher values of the superpotential coupling λ_S [hence larger λ_T, as $\lambda_T = \lambda_S\tan\theta_W$ (θ_W being the usual weak

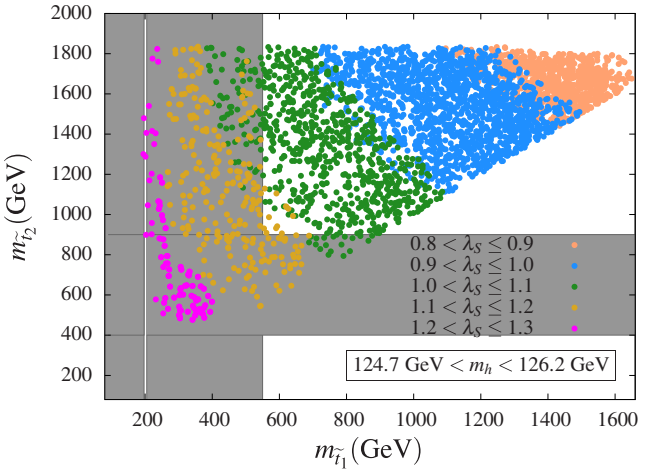

FIG. 1. Allowed region in the $(m_{\tilde{t}_1} - m_{\tilde{t}_2})$ plane compatible with 124.7 GeV $< m_h <$ 126.2 GeV Higgs mass after taking into consideration the full one-loop corrections. The grey bands indicate the values of $m_{\tilde{t}_1}$ and $m_{\tilde{t}_2}$ ruled out by the LHC (see text for more details). The narrow vertical strip over 197 GeV $\lesssim m_{\tilde{t}_1} \lesssim$ 205 GeV refers to the stealth top squark regime.

[2]See Refs. [22,45] for a detailed discussion.

mixing angle) chosen to fit the neutrino mass at the tree level] provide larger corrections to the Higgs boson mass at the loop level and hence the requirement of having multi-TeV top squarks can be avoided. The largest values considered for $m_{\tilde{t}_1}$ and $m_{\tilde{t}_2}$ in this plot are close to 1660 and 1830 GeV, respectively.

As can be seen from this figure, relatively light top squarks with $m_{\tilde{t}_1} \simeq m_{\tilde{t}_2}$ may be generic to our scenario (though such a situation could attract more aggressive constraints from the LHC). Furthermore, both of them can have sub-TeV masses simultaneously and can still be consistent with the observed value of the SM-like Higgs mass if $\lambda_S > 1$. In the absence of any appreciable chiral mixing [left-right ($L-R$) mixing], top squarks as heavy as values considered here could only raise the Higgs boson mass up to around 114 GeV in the MSSM. Hence the model under consideration has a very interesting and distinct feature where light to moderately heavy (∼1 TeV) top squarks with negligible $L-R$ mixing can be compatible with the observed mass of the Higgs boson. Similar possibilities are discussed earlier in generic setups [76] and more recently, in a specific SUSY scenario like the next-to-minimal SUSY extension of the SM [77].

Taking advantage of this situation, we explore relatively light top squarks satisfying the relevant direct search constraints. We further note that a top squark within a narrow mass window between 197 and 205 GeV [78], which is still allowed by data from the 8 TeV run of the LHC, can be obtained in our scenario for $\lambda_S \geq 1.2$. Such a mass window with $m_{\tilde{t}} \gtrsim m_t$ is known in the literature as the stealth window [79–83] for the top squark when the carriers of MET are extremely light (as with the neutrinos in the cascade of the SM top quark). This renders the signal characteristics of the top squark rather similar to that of the top quark thus making the presence of the former in the data difficult to recognize. Given that the model we consider indeed bears superlight carriers of MET (as we will discuss in Sec. IV A), such a stealth scenario can be easily accommodated in our scenarios. Precise measurements of the SM top quark properties such as its pair-production cross section could offer probe to the stealth top squark scenario. Equivalently, the presence of a light top squark may also have some impact on the measurements of the top quark mass [84]. We briefly touch upon the situation with such stealth top squarks in Sec. VIII.

IV. THE ELECTROWEAK GAUGINOS

In this section we discuss issues pertaining to neutrino masses and the fermionic sector of the scenario. These will help us understand the effect of large neutrino Yukawa coupling (f) in the present context. The electroweak gauginos are comprised of the neutralinos and charginos. However, contrary to the MSSM scenario, the neutralinos are Dirac fermions in the R-preserving case. In the R-breaking case they take a pseudo-Dirac form, in general.

A. The neutralino sector

The decay branching fractions in various available final states of the top squarks depend crucially on the neutralino sector. The neutralino sector in this model differs from that of the MSSM due to the presence of additional fermionic fields such as $\tilde{S}$, $\tilde{T}^0$, $\tilde{R}_d^0$. In addition, due to the non-vanishing sneutrino VEV, the active neutrino mixes with the neutralinos. Let us first discuss the neutralino mass matrix in the R-preserving scenario, although, ultimately we carry out our analysis by considering a mild R-symmetry violation. This opens up several new and interesting phenomenological issues, which we will mention in due course.

1. The R-conserving case

The part of the Lagrangian that corresponds to the neutral fermion mass matrix is given by $\mathcal{L} = (\psi^{0+})^T M_\chi^D (\psi^{0-})$ where $\psi^{0+} = (\tilde{b}^0, \tilde{w}^0, \tilde{R}_d^0, N^c)$ and $\psi^{0-} = (\tilde{S}, \tilde{T}^0, \tilde{H}_u^0, \nu_e)$. The superscript ($\pm$) indicates the respective R charges which are $+1$ and -1. The neutral Dirac fermion mass matrix M_χ^D is given by [52]

$$M_\chi^D = \begin{pmatrix} M_1^D & 0 & \frac{g' v_u}{\sqrt{2}} & -\frac{g' v_a}{\sqrt{2}} \\ 0 & M_2^D & -\frac{g v_u}{\sqrt{2}} & \frac{g v_a}{\sqrt{2}} \\ \lambda_S v_u & \lambda_T v_u & \mu_u + \lambda_S v_S + \lambda_T v_T & 0 \\ M_R & 0 & -f v_a & -f v_u \end{pmatrix}. \quad (10)$$

The Dirac neutralino mass matrix can be diagonalized by a biunitary transformation involving two unitary matrices V^N and U^N. The resulting four Dirac mass eigenstates are $\tilde{\chi}_i^{0+} \equiv \begin{pmatrix} \tilde{\psi}_i^{0+} \\ \tilde{\psi}_i^{0-} \end{pmatrix}$, with $i = 1, 2, 3, 4$ and $\tilde{\psi}_i^{0+} = V_{ij}^N \psi_j^{0+}$, $\tilde{\psi}_i^{0-} = U_{ij}^N \psi_j^{0-}$. With certain simplifying assumptions [52] and with

$$\lambda_T = \lambda_S \tan\theta_W, \qquad M_R = \frac{\sqrt{2} f M_1^D \tan\beta}{g \tan\theta_W}, \quad (11)$$

the expression for the mass of the lightest neutralino state ($\tilde{\chi}_1^0$), i.e., the Dirac neutrino reduces to [52]

$$m_{\nu_e}^D = \frac{v^3 f g \sin\beta}{\sqrt{2}(\mu_u + \lambda_S v_S + \lambda_T v_T)} \lambda_T \frac{(M_2^D - M_1^D)}{M_1^D M_2^D}. \quad (12)$$

Note that only ν_e acquires a mass at the tree level since only the electron-type sneutrino gets a nonzero VEV. By choosing nearly degenerate Dirac masses for the electroweak gauginos, i.e., ($M_2^D - M_1^D \simeq 0.1$ GeV) one can find from Eq. (12) that the Dirac neutrino mass can be in the right ballpark of 0.1 eV even when $f \sim \mathcal{O}(1)$ and assuming M_1^D, M_2^D and μ_u to be close to a few hundred GeV. The requirement of such a

degeneracy between the Dirac masses of the electroweak gauginos, however, could be relaxed if one can consider an appropriately small $\lambda_T \sim 10^{-6}$ [52]. However, a small λ_T is not so interesting for our purpose since this results in a diminished contribution to m_h and thus, brings back the scenario with multi-TeV top squarks to have the Higgs boson mass at the right ballpark. At colliders, a direct attempt to probe this connection would inevitably involve the heavy right handed neutrino (N_R) coupling to an active neutrino (ν_e) and the SM-like Higgs boson. However, while a larger value of f enhances this coupling, this also pushes up the mass of the right handed neutrino, as conspicuous from Eq. (11). We find that it is rather difficult to obtain $m_{N_R} \leq 1.5$ TeV in a consistent manner while keeping $f \sim \mathcal{O}(1)$. An immediate probe to this at the LHC can be the electroweak process $pp \to N_R e^+ h$ followed by N_R decaying to $h\nu_e$ thus giving rise to a final state $\nu_e e^+ hh$. Our preliminary study reveals that the corresponding rate could barely reach an attobarn level at the 13 TeV run of the LHC and thus one needs to wait for a very high integrated luminosity. A detailed analysis in this context is beyond the scope of this paper and we postpone it for a future work [85].

2. The R-breaking case

In the context of a supergravity theory broken spontaneously in the hidden sector, we consider R symmetry to be broken by a nonzero gravitino mass. The R-breaking information has to be communicated from the hidden sector to the visible sector. We choose anomaly mediated supersymmetry breaking to play the role of a messenger [39,52]. The R-breaking Lagrangian contains the following terms

$$\begin{aligned}\mathcal{L}_{\not R} = {} & M_1 \tilde{b}^0 \tilde{b}^0 + M_2 \tilde{w}^0 \tilde{w}^0 + M_3 \tilde{g}\,\tilde{g} + \sum_{b=2,3} A^l_b \tilde{L}_a \tilde{L}_b \tilde{E}^c{}_b + \sum_{k=1,2,3} A^d_k \tilde{L}_a \tilde{Q}_k \tilde{D}^c{}_k \\ & + \sum_{k=1,2,3} \frac{1}{2} A^\lambda_{23k} \tilde{L}_2 \tilde{L}_3 \tilde{E}^c{}_k + \sum_{j,k=1,2,3;b=2,3} A^{\lambda'}_{bjk} \tilde{L}_b \tilde{Q}_j \tilde{D}^c{}_k + A^\nu H_u \tilde{L}_a \tilde{N}^c + H_u \tilde{Q} A^u \tilde{U}^c, \end{aligned} \tag{13}$$

where, M_1, M_2 and M_3 are the Majorana masses corresponding to $U(1)$, $SU(2)$ and $SU(3)$ gauginos, respectively. The A terms are the standard trilinear scalar couplings. For the rest of this work, we will consider the R-breaking effects to be small, parametrized in terms of the gravitino mass considered to be roughly ∼20 GeV.

The Majorana neutralino mass matrix containing R-breaking effects can be written in the basis $\psi^0 = (\tilde{b}^0, \tilde{S}, \tilde{w}^0, \tilde{T}, \tilde{R}_d, \tilde{H}^0_u, N^c, \nu_e)^T$ as

$$\mathcal{L}^{\rm mass}_{\tilde{\chi}^0} = \frac{1}{2} (\psi^0)^T M^M_\chi \psi^0 + \text{H.c.} \tag{14}$$

The symmetric 8×8 neutralino mass matrix M^M_χ is given by

$$M^M_\chi = \begin{pmatrix} M_1 & M^D_1 & 0 & 0 & 0 & \frac{g' v_u}{\sqrt{2}} & 0 & -\frac{g' v_a}{\sqrt{2}} \\ M^D_1 & 0 & 0 & 0 & \lambda_S v_u & 0 & M_R & 0 \\ 0 & 0 & M_2 & M^D_2 & 0 & -\frac{g v_u}{\sqrt{2}} & 0 & \frac{g v_a}{\sqrt{2}} \\ 0 & 0 & M^D_2 & 0 & \lambda_T v_u & 0 & 0 & 0 \\ 0 & \lambda_S v_u & 0 & \lambda_T v_u & 0 & \mu_u + \lambda_S v_S + \lambda_T v_T & 0 & 0 \\ \frac{g' v_u}{\sqrt{2}} & 0 & -\frac{g v_u}{\sqrt{2}} & 0 & \mu_u + \lambda_S v_S + \lambda_T v_T & 0 & -f v_a & 0 \\ 0 & M_R & 0 & 0 & 0 & -f v_a & 0 & -f v_u \\ -\frac{g' v_a}{\sqrt{2}} & 0 & \frac{g v_a}{\sqrt{2}} & 0 & 0 & 0 & -f v_u & 0 \end{pmatrix}. \tag{15}$$

This can be diagonalized by a unitary transformation

$$N^\star M^M_\chi N^\dagger = (M_\chi)_{\rm diag}. \tag{16}$$

We define the two-component mass eigenstates as

$$\chi^0_i = N_{ij} \psi^0_j, \qquad i, j = 1, \ldots, 8. \tag{17}$$

Finally the four-component Majorana spinors in terms of the two-component states are defined as

$$\tilde{\chi}_i^0 = \begin{pmatrix} \chi_i^0 \\ \bar{\chi}_i^0 \end{pmatrix}, \qquad i = 1, \ldots 8. \tag{18}$$

The lightest state ($\tilde{\chi}_1^0$), which is the neutrino, becomes a Majorana particle. Similar to the Dirac case, the lightest eigenvalue of this Majorana neutralino mass matrix resembles the mass of the active neutrino. The other two active neutrinos remain massless at this stage. Using the relationships between λ_S and λ_T as well as M_R and f as shown in Sec. IV A 1, the mass of the active neutrino can be expressed as [52]

$$(m_\nu)_{\text{Tree}} = -v^2 \frac{[g\lambda_T v^2 (M_2^D - M_1^D)\sin\beta]^2}{[M_1\alpha^2 + M_2\delta^2]}, \tag{19}$$

where

$$\begin{aligned} \alpha &= \frac{2M_1^D M_2^D(\mu_u + \lambda_S v_S + \lambda_T v_T)\tan\beta}{g\tan\theta_w} \\ &\quad + \sqrt{2}v^2\lambda_S \tan\beta(M_1^D \sin^2\beta + M_2^D \cos^2\beta), \\ \delta &= \sqrt{2}M_1^D v^2 \lambda_T \tan\beta. \end{aligned} \tag{20}$$

It is noteworthy that the parameter λ_T not only gives a tree level mass to the neutrinos but also helps lift the Higgs mass through quartic terms generated at one-loop level. For example, we have observed that the tree level Majorana mass of the active neutrino varies from 0.09 to 0.23 eV when λ_T varies in the range 0.8–1.3, used in Fig. 1, which gives correct SM-like Higgs mass (∼125 GeV) when top squarks are also not too heavy. Also note that the neutrino Majorana mass given in Eq. (19) does not depend on the neutrino Yukawa coupling f. This is because the expression has the functional form M_R/f. Since $M_R \sim f$ therefore, the neutrino Majorana mass becomes devoid of f. Similar to the case of Dirac neutrino mass, an appropriately small Majorana mass of the active neutrino requires highly degenerate Dirac gaugino masses. Note that [Eq. (19)] the neutrino Majorana mass is independent of the neutrino Yukawa coupling f. This is in clear contrast to the Dirac case. However, by choosing appropriate values of other parameters one can obtain a light active neutrino ($\tilde{\chi}_1^0$) with mass 0.1 eV. Nevertheless, some interesting observations can be made for various sizes of f. For example, $f \sim \mathcal{O}(10^{-4})$ gives a sterile neutrino with mass around a few keV [58] which can be accommodated as a dark matter candidate. On the other hand, for $f \sim \mathcal{O}(1)$, where we obtain a large tree level correction to the Higgs boson mass for low values of $\tan\beta$, a light bino-like neutralino ($\tilde{\chi}_2^0$) with mass around a few hundred MeV (mass of this neutralino is mostly controlled by the R-breaking parameter M_1). This MeV neutralino LSP could decay to SM fermions via R-parity violating modes. The probable decay modes could be $\tilde{\chi}_2^0 \to q\bar{q}\nu$, $e^+e^-\nu$, $\nu\nu\nu$, $q\bar{q}'e^-$, where q, q' are the SM light quark states from the first two generations. However, as these involve very small couplings thus resulting in small total decay widths, the decay lengths happen to be much larger than the collider dimension [72]. As a result, the LSP neutralino contributes to MET signals. Furthermore, the gravitino NLSP (∼20 GeV) would decay to a photon and the bino-like LSP neutralino. This affects the light element abundances which are strongly constrained observationally and results in an upper bound on the reheating temperature of the Universe $T_R \leq 10^8$ GeV [86]. In our scenario, one of the active neutrinos acquires a mass at the tree level. In addition, there are one-loop contributions to the neutrino Majorana mass matrix. We observe that in this model and for our benchmark points, the one-loop contributions involving the $b - \tilde{b}$, $\tau - \tilde{\tau}$ loop interfere destructively with the Higgs-neutralino loop resulting in a somewhat relaxed bound (∼20 GeV) on the gravitino mass. This cancellation occurs for $(m_\nu)_{11}$ where the Higgs-neutralino loop is present. For other elements in the neutrino mass matrix we obtain a bound on the relevant RPV operators [52]. This cancellation was not considered previously [34,39] and as a result a stronger bound on gravitino mass was obtained. We have also implemented the model in SARAH 4.4.1, which performs a full one-loop correction to the neutralino mass matrix, and we have cross-checked with the spectrum file that gravitino mass in the ballpark of $\mathcal{O}(10)$ GeV is consistent with light neutrino masses and mixing.

B. The chargino sector

Just like the neutrino and the neutralinos would mix, the charged lepton mixes[3] with the charginos. This results in an extended chargino mass matrix [63] compared to the MSSM. The relevant Lagrangian after R breaking consists of the following terms

$$\begin{aligned} \mathcal{L}_{ch} &= M_2\tilde{w}^+\tilde{w}^- + (M_2^D - gv_T)\tilde{T}_d^-\tilde{w}^+ + \sqrt{2}\lambda_T v_u \tilde{T}_u^+\tilde{R}_d^- \\ &\quad + gv_u\tilde{H}_u^+\tilde{w}^- - \mu_u\tilde{H}_u^+\tilde{R}_d^- + \lambda_T v_T\tilde{H}_u^+\tilde{R}_d^- - \lambda_S v_S\tilde{H}_u^+\tilde{R}_d^- \\ &\quad + gv_a\tilde{w}^+e_L^- + (M_2^D + gv_T)\tilde{T}_u^+\tilde{w}^- + m_e e_R^c e_L^- + \text{H.c.} \end{aligned} \tag{21}$$

The 4×4 chargino mass matrix written in the basis $\psi_i^+ = (\tilde{w}^+, \tilde{T}_u^+, \tilde{H}_u^+, e_R^c)^T$ and $\psi_i^- = (\tilde{w}^-, \tilde{T}_d^-, \tilde{R}_d^-, e_L^-)^T$ is given by

[3]The mixing between the charged leptons and the charginos gives rise to deviation of the Z to charged lepton couplings. Such a deviation is very much constrained from the electroweak precision measurements leading to a lower bound on $\tan\beta \geq 2.7$ [34,45]. It is also pertinent to mention that an upper bound on $\tan\beta$ comes from τ Yukawa coupling contributing to the ratio $R_\tau \equiv \Gamma(\tau \to e\bar{\nu}_e\nu_\tau)/\Gamma(\tau \to \mu\bar{\nu}_\mu\nu_\tau)$ [34,45]. Choosing $m_{\tilde{\tau}_R}$ to be around 1 TeV corresponds to $\tan\beta \leq 70$.

$$M_c = \begin{pmatrix} M_2 & M_2^D - g v_T & 0 & g v_a \\ M_2^D + g v_T & 0 & \sqrt{2} v_u \lambda_T & 0 \\ g v_u & 0 & -\mu_u - \lambda_S v_S + \lambda_T v_T & 0 \\ 0 & 0 & 0 & m_e \end{pmatrix}. \tag{22}$$

Again, this can be diagonalized by a biunitary transformation $UM_cV^T = M_D^{\pm}$. The chargino mass eigenstates (two component) are written in terms of the gauge eigenstates in a compact form as

$$\chi_i^- = U_{ij}\psi_j^-, \qquad \chi_i^+ = V_{ij}\psi_j^+. \tag{23}$$

The four-component Dirac spinors written in terms of the two-component spinors take the form

$$\tilde{\chi}_i^+ = \begin{pmatrix} \chi_i^+ \\ \bar{\chi}_i^- \end{pmatrix}, \qquad (i = 1, \ldots, 4). \tag{24}$$

The lightest chargino ($\tilde{\chi}_1^-$) corresponds to the electron; $\tilde{\chi}_2^-$ is the lightest chargino state reminiscent of the lighter chargino in the MSSM with mass of $\mathcal{O}(100)$ GeV. It is also pertinent to mention that ψ_i^- and ψ_i^+ would also include μ_L^-, τ_L^- and μ_R^c, τ_R^c, respectively. However, as discussed in Sec. II only the electron-type sneutrino acquires a VEV, and the VEV of the other two sneutrinos can be rotated away without any loss of generality. Therefore, μ and τ do not mix with the chargino states.

V. THE TOP SQUARK SECTOR

In this work we concentrate on the third generation squarks, mainly the top squarks, which play important roles in lifting the Higgs boson mass. Scenarios with light top squarks draw their motivations from the naturalness argument. They also provide rich and interesting collider signatures. As discussed in Sec. III, the model which we consider here gives us the opportunity to study such light top squarks. Furthermore, R symmetry prohibits any trilinear scalar couplings (the A terms) and Higgsino mass parameter (the μ term). Therefore, we investigate a situation where both the top squarks are light (∼500 GeV) and have negligible chiral mixing, which originates from small R breaking.

The relevant terms in the top squark mass matrix are generated from the F term, the D term and the soft terms. The $SU(2)_L$ and $U(1)_Y$ contributions to the D fields are given by

$$\begin{aligned} D^a &= g[H_u^\dagger \tau^a H_u + \tilde{L}_i^\dagger \tau^a \tilde{L}_i + \tilde{q}_{iL}^\dagger \tau^a \tilde{q}_{iL} + T^\dagger \lambda^a T] + \sqrt{2}[M_2^D T^a + M_2^D T^{a\dagger}], \\ D^Y &= -\frac{1}{2} g' \left[H_u^\dagger H_u - \tilde{L}_i^\dagger \tilde{L}_i + 2\tilde{e}_{iR}^* e_{iR} + \frac{1}{3}\tilde{q}_{iL}^\dagger \tilde{q}_{iL} - \frac{4}{3}\tilde{u}_{iR}^\dagger u_{iR} + \frac{2}{3}\tilde{d}_{iR}^\dagger \tilde{d}_{iR} \right] \\ &\quad - \sqrt{2} M_1^D [S + S^\dagger]. \end{aligned} \tag{25}$$

The τ and λ matrices are the generators of the $SU(2)_L$ group in the fundamental and adjoint representation, respectively. From Eq. (25) it is straightforward to calculate the elements of the mass-squared matrix in the top squark sector, which in the basis $(\tilde{t}_L, \tilde{t}_R)$ turn out to be

$$\begin{aligned} (M_{\tilde{t}}^2)_{11} &= m_{\tilde{Q}_3}^2 + m_t^2 + m_Z^2 \cos 2\beta \left(\frac{1}{2} - \frac{2}{3}\sin^2\theta_W \right) + \frac{\sqrt{2}}{3} v_S M_1^D + \sqrt{2} g M_2^D v_T, \\ (M_{\tilde{t}}^2)_{12} &= (M_{\tilde{t}}^2)_{21} = 0, \\ (M_{\tilde{t}}^2)_{22} &= m_{\tilde{u}_3}^2 + m_t^2 + \frac{2}{3} m_Z^2 \sin^2\theta_W \cos 2\beta - \frac{4\sqrt{2}}{3} g' M_1^D v_S. \end{aligned} \tag{26}$$

Note that in absence of A terms and the μ term, the off-diagonal entries vanish and hence the top squark sector is devoid of any chiral mixing. Thus, the left- and right-chiral states are equivalent to the mass eigenstates. Such a "zero" mixing situation can be contrasted with the MSSM, in which a substantial mixing is generally required to obtain the observed value of the Higgs mass. Motivated by the recent collider bounds on the masses of the top squarks (depending on its various decay modes), to be justified in some detail in Sec. V C, we choose $\tilde{t}_1 \approx \tilde{t}_R$ and $\tilde{t}_2 \approx \tilde{t}_L$.

At the LHC, top squarks are being searched in their direct production, $pp \to \tilde{t}\tilde{t}^*$, followed by their subsequent decays in various possible modes. Out of these, the decays that are relevant to our scenario [87–90] are the R-parity conserving ones

$$\tilde{t} \to b\tilde{\chi}^+ \quad \text{and} \quad \tilde{t} \to t\tilde{\chi}^0, \tag{27}$$

and the modes that violate R parity when a top squark could decay to a bottom quark and a charged lepton [91,92]

$$\tilde{t} \to b\ell^+. \tag{28}$$

These channels are of major relevance in the context of our model. The reasons are twofold: First, in the large f scenario, we obtain a light bino-like neutralino with mass around a few hundred MeV, in addition to an active neutrino. Therefore, the channels with top squark decaying to a top quark and a bino-like neutralino and/or an active neutrino open up. Second, a top squark decaying to a bottom quark and a chargino is also important. Additionally, a top squark decaying to a bottom quark and an electron becomes an interesting channel to look for. This decay mode is predominantly controlled by the R-parity violating operator λ'_{133}. In the framework of the MSSM with R-parity violation, a strong limit on this particular coupling exists from the neutrino Majorana mass, $|\lambda'_{133}| \sim 3.4 \times 10^{-3}\sqrt{\frac{m_b}{m_{\tilde{b}}}}$ [93]. Hence, in such a scenario, the resulting decay rate becomes highly suppressed. However, in the present context, λ'_{133} is identified with the bottom Yukawa coupling y_b. The smallness of the neutrino mass is then explained through a small R-breaking effect parametrized in terms of a small gravitino mass [52]. Thus, a large decay rate for $\tilde{t} \to be^+$ becomes a generic feature in our model. In principle, $\tilde{t}$ could also decay to $b\mu^+$ and $b\tau^+$ via RPV couplings λ'_{233} and λ'_{333}. However, these decays are subdominant compared to $\tilde{t} \to be^+$ because of the stringent constraints on the relevant couplings as discussed later. We note in passing that $\tilde{t} \to t\tilde{G}$ is also a possibility but highly suppressed [94] for a gravitino of mass ~20 GeV in the present context.

The relevant Lagrangians are worked out in the four-component notation following [95,96] and are given by

$$\mathcal{L}_{\tilde{t}t\tilde{\chi}_0} = -\bar{t}\left[y_t P_L N_{i6} + \frac{1}{\sqrt{2}}\left\{gP_R N_{i3} + \frac{g'}{3}P_R N_{i1}\right\}\right]\tilde{t}_L\tilde{\chi}_i^0 + \bar{t}\left[\frac{4g'}{3\sqrt{2}}P_L N_{i1} - y_t P_R N_{i6}\right]\tilde{t}_R\tilde{\chi}_i^0 + \text{H.c.} \tag{29}$$

and

$$\mathcal{L}_{\tilde{t}b\tilde{\chi}^+} = \bar{b}[-gP_L U_{i1}]\tilde{t}_L\tilde{\chi}_i^c + \bar{b}[y_t P_R V_{i3}]\tilde{t}_R\tilde{\chi}_i^c + \lambda'_{133}\tilde{t}_L P_L U_{i4}\tilde{\chi}_i^c\bar{b} + \text{H.c.}, \tag{30}$$

where $\lambda'_{133} = y_b = \frac{m_b}{v\cos\beta}$, the bottom Yukawa coupling and $y_t = \frac{m_t}{v\sin\beta}$ is the top Yukawa coupling and m_t and m_b are the top and the bottom quark masses, respectively. The neutralino and the chargino mixing matrices N_{ij}, U_{ij} and V_{ij} are as defined earlier. Note that for $i = 1$ (corresponding to $\tilde{\chi}_i^c \equiv e^-$) the mixing matrix elements U_{11} and V_{13} are suppressed. In the following subsections we briefly discuss the salient decay modes of the lighter ($\tilde{t}_1 \approx \tilde{t}_R$) and the heavier ($\tilde{t}_2 \approx \tilde{t}_L$) top squarks.

A. Decay rates of $\tilde{t}_1(\approx \tilde{t}_R)$

The partial decay widths of $\tilde{t}_1$ in the $t\tilde{\chi}_i^0$ and $b\tilde{\chi}_i^+$ modes are given by

$$\Gamma(\tilde{t}_1 \to t\tilde{\chi}_i^0) = \frac{1}{16\pi m_{\tilde{t}_1}^3}[(\eta_{Ri}^2 + \zeta_{Ri}^2)(m_{\tilde{t}_1}^2 - m_t^2 - m_{\tilde{\chi}_i^0}^2) - 4\eta_{Ri}\zeta_{Ri}m_t m_{\tilde{\chi}_i^0}] \times [m_{\tilde{t}_1}^4 + m_{\tilde{\chi}_i^0}^4 + m_t^4 - 2m_{\tilde{t}_1}^2 m_t^2 - 2m_{\tilde{\chi}_i^0}^2 m_t^2 - 2m_{\tilde{\chi}_i^0}^2 m_{\tilde{t}_1}^2]^{\frac{1}{2}} \tag{31}$$

and

$$\Gamma(\tilde{t}_1 \to b\tilde{\chi}_i^+) = \frac{1}{16\pi m_{\tilde{t}_1}^3}[(\alpha_{Ri}^2 + \beta_{Ri}^2)(m_{\tilde{t}_1}^2 - m_b^2 - m_{\tilde{\chi}_i^+}^2) - 4\alpha_{Ri}\beta_{Ri}m_b m_{\tilde{\chi}_i^+}] \times [m_{\tilde{t}_1}^4 + m_{\tilde{\chi}_i^+}^4 + m_b^4 - 2m_{\tilde{t}_1}^2 m_b^2 - 2m_{\tilde{\chi}_i^+}^2 m_b^2 - 2m_{\tilde{\chi}_i^+}^2 m_{\tilde{t}_1}^2]^{\frac{1}{2}}, \tag{32}$$

where

$$\eta_{Ri} = \frac{4g'}{3\sqrt{2}}N_{i1}, \quad \zeta_{Ri} = y_t N_{i6}, \quad \alpha_{Ri} = 0, \quad \beta_{Ri} = y_t V_{i3}. \tag{33}$$

We note down a few important observations below.

(i) In the large f case we obtain a light (~ few hundred MeV governed by the R-breaking Majorana mass M_1) bino-like neutralino ($\tilde{\chi}_2^0$). This is because of the presence of the $M_R N^c \tilde{S}$ term in the Lagrangian, where the coefficient M_R becomes very large ($\sim 10^5$ GeV) for an order one f. This results in forming a heavy pseudo-Dirac pair with mass $\sim M_R$ and makes the lightest eigenvalue very small and predominantly bino-like.

(ii) The Dirac wino mass M_2^D is considered to be heavy to evade bounds from Z boson coupling to electrons [45] (see also Sec. IV B). The μ_u parameter, which

controls the mass of the Higgsino (both neutral and charged) can vary between the electroweak scale (∼200 GeV) and a much larger value, i.e., a few TeV.

(iii) Based on the above discussion and with the help of Eqs. (29)–(33), we find that $\tilde{t}_1$ would decay into $t\tilde{\chi}^0_{2,3,4}$ and $b\tilde{\chi}^+_2$. The neutralino can be both bino- or Higgsino-like whereas the chargino would only be Higgsino-like, assuming the Higgsino mass parameter $\mu_u (< m_{\tilde{t}_1}) \ll M_2^D$.

(iv) We expect the dominant decay modes of $\tilde{t}_1$ to have the Higgsino-like neutralinos or chargino as the decay products rather than the bino-like neutralino. This is because of the enlarged couplings for the former which are proportional to the top Yukawa coupling, y_t.

(v) Finally, in the limit when $\mu_u > m_{\tilde{t}_1}$, the top squark cannot decay to an on-shell top quark and a Higgsino-like neutralino or a bottom quark and a Higgsino-like chargino due to phase space constraints. Therefore, the dominant channel would only be $\tilde{t}_1 \to t\tilde{\chi}^0_2$, where $\tilde{\chi}^0_2$ is the bino-like MeV neutralino. Moreover, $\tilde{t}_1 \to t\nu_e$ would also contribute to MET, although the branching is suppressed due to the small neutralino-neutrino mixing.

B. Decay rates of $\tilde{t}_2 (\approx \tilde{t}_L)$

The partial decay widths of $\tilde{t}_2$ are given by

$$\Gamma(\tilde{t}_2 \to t\tilde{\chi}^0_i) = \frac{1}{16\pi m^3_{\tilde{t}_2}}[(\eta^2_{Li}+\zeta^2_{Li})(m^2_{\tilde{t}_2}-m^2_t-m^2_{\tilde{\chi}^0_i})-4\eta_{Li}\zeta_{Li}m_t m_{\tilde{\chi}^0_i}] \times [m^4_{\tilde{t}_2}+m^4_{\tilde{\chi}^0_i}+m^4_t-2m^2_{\tilde{t}_2}m^2_t-2m^2_{\tilde{\chi}^0_i}m^2_t-2m^2_{\tilde{\chi}^0_i}m^2_{\tilde{t}_2}]^{\frac{1}{2}} \quad (34)$$

and

$$\Gamma(\tilde{t}_2 \to b\tilde{\chi}^+_i) = \frac{1}{16\pi m^3_{\tilde{t}_2}}[(\alpha^2_{Li}+\beta^2_{Li})(m^2_{\tilde{t}_2}-m^2_b-m^2_{\tilde{\chi}^+_i})-4\alpha_{Li}\beta_{Li}m_b m_{\tilde{\chi}^+_i}] \times [m^4_{\tilde{t}_2}+m^4_{\tilde{\chi}^+_i}+m^4_b-2m^2_{\tilde{t}_2}m^2_b-2m^2_{\tilde{\chi}^+_i}m^2_b-2m^2_{\tilde{\chi}^+_i}m^2_{\tilde{t}_2}]^{\frac{1}{2}}, \quad (35)$$

where

$$\eta_{Li} = y_t N_{i6}, \quad \zeta_{Li} = \frac{1}{\sqrt{2}}\left(gN_{i3}+\frac{g'}{3}N_{i1}\right), \quad \alpha_{Li} = -gU_{i1}, \quad \beta_{Li} = 0. \quad (36)$$

In addition, for $\tilde{t}_2$ we also have the interesting possibility of $\tilde{t}_2 \to be^+$. The corresponding partial decay width is given by

$$\Gamma(\tilde{t}_2 \to be^+) = \frac{y^2_b |U_{i4}|^2}{16\pi} m_{\tilde{t}_2}. \quad (37)$$

Some features of $\tilde{t}_2$ decays are as follows:

(i) The decay $\tilde{t}_2 \to be^+$ is an interesting possibility. This faces no suppression from the phase space and the decay rate is proportional to the bottom Yukawa coupling, y_b which grows with $\tan\beta$. Hence a substantial branching fraction in this mode is expected at large $\tan\beta$ and for a fixed top squark mass.

(ii) When $\mu_u < m_{\tilde{t}_2}$, $\tilde{t}_2$ would decay to a Higgsino-like chargino and neutralinos. Also, decay to a bino-like neutralino is a possibility. However, a quick look at the couplings in Eq. (36) would suggest that the decay to Higgsino-like neutralinos ($\tilde{\chi}^0_3$, $\tilde{\chi}^0_4$) is $\eta_{Li} \sim y_t$ enhanced and hence, is more probable than a decay to a bino-like neutralino (suppressed by $g'/3$ in the coupling) or to a Higgsino-like chargino (suppressed by g times the wino component of the lighter chargino, U_{i1}).

(iii) Again, for $\mu_u > m_{\tilde{t}_2}$, decays of $\tilde{t}_2$ to Higgsino-like neutralinos and charginos are kinematically barred. Under such a circumstance, $\tilde{t}_2$ mainly decays to a bottom quark and an electron (positron). The decay mode $\tilde{t}_2(\tilde{t}_L) \to t\tilde{\chi}^0_2$ is again suppressed because of a (comparatively) small involved coupling. Finally, $\alpha_{Ri} = \beta_{Li} = 0$ reflects the absence of $\hat{H}_d$ in the Lagrangian, which has been integrated out from the theory.

C. Bounds on top squarks

(i) Recently ATLAS measured the spin correlation in the top-antitop quark events and searched for top squark pair production [97] in the pp collisions at $\sqrt{s} = 8$ TeV center-of-mass energy and integrated luminosity ($\mathcal{L}$) of 20.3 fb^{-1}. This particular search has ruled out top squarks with masses between the top quark mass and 191 GeV with 95% confidence level. A very recent study [78] reveals that the window of 197 GeV $\lesssim m_{\tilde{t}_1} \lesssim$ 205 GeV, in the so-called stealth regime (i.e., with vanishing LSP mass) cannot yet be ruled out.

(ii) Dedicated searches for pair-produced top squarks decaying 100% of the time to bottom quarks and lighter charginos have been performed [98,99] within the framework of the MSSM. For a chargino with mass close to 200 GeV, the top squark below 470 GeV has been ruled out at the $\sqrt{s} = 8$ TeV run of the LHC. In our scenario, $\tilde{t}_R$ decays to this particular channel if $\mu_u < m_{\tilde{t}_R}$. Although in our model corresponding branching ratio (BR) is less

than 100%, we take a conservative approach and respect this bound. In addition, this search gives the most relaxed bound on the mass of the top squark which is relevant to our analysis. Hence in the present study we choose $\tilde{t}_R$ to be the lighter top squark, i.e., $\tilde{t}_1 \approx \tilde{t}_R$.

(iii) Another decay mode of the top squark relevant to our scenario is $\tilde{t} \to t\tilde{\chi}_1^0$, where $\tilde{\chi}_1^0$ implies the lightest supersymmetric particle in the MSSM (in our work, however, $\tilde{\chi}_1^0$ is identified with the active neutrino and $\tilde{\chi}_2^0$ represents the lightest bino-like neutralino). At the 8 TeV run of the LHC, a top squark with mass below 550 GeV is ruled out at 95% confidence level [98,99] with the assumption $\mathrm{BR}(\tilde{t}_1 \to t\tilde{\chi}_1^0) = 100\%$. This bound applies for a massless neutralino ($m_{\tilde{\chi}_1^0} = 0$). For heavier neutralinos in the final states, this lower bound on the top squark mass can be relaxed further. Note that in the large f scenario we find a light superlight bino-like neutralino with mass around a few hundred MeV which thus attracts this bound on the mass of the lighter top squark.

(iv) A top squark decaying via R-parity violating mode has also been probed by the LHC experiments. If a top squark undergoes an R-parity violating decay only to a bottom quark and an electron, a stringent lower bound [91,92] exists on the top squark mass with $m_{\tilde{t}} > 900$ GeV.[4] Accommodating an even lighter top squark, which is central to our present work, thus requires a situation where such a bound is preferentially applicable to the heavier top squark state ($\tilde{t}_2$) of the scenario. As described in Sec. V B, only $\tilde{t}_L$ could decay to a bottom quark and an electron (positron). Hence we choose the heavier top squark $\tilde{t}_2$ to be the $\tilde{t}_L$, i.e., $\tilde{t}_2 \approx \tilde{t}_L$. Note again that our consideration is pretty conservative and, as we would find in Sec. VI, for generic scenarios where such a decay can have a branching fraction below 50%, the bounds can get considerably weaker thus allowing for an even lighter $\tilde{t}_2$. Phenomenological discussions on top squarks undergoing such an R-parity violating decay can be found in Refs. [101–107].

The squarks from the third generation have understandably attracted a lot of attention in the recent times. The flavor changing decay of the top squark $\tilde{t}_1 \to c\tilde{\chi}_1^0$ has been analyzed in great detail in [77,108–111]. Recent searches performed by both ATLAS and CMS collaborations have looked into this channel extensively and ruled out top squark masses below 300 GeV [78,112,113]. Top squarks decaying to a top quark along with a neutralino (LSP or next-to-lightest SUSY particle (NLSP)) have also been probed in various SUSY models. A lower limit close to 1 TeV for the top squark mass can be obtained at $\sqrt{s} =$ 14 TeV and with the high luminosity option [114–116]. In addition, thorough phenomenological studies have also been performed in the decay of top squark into a bottom quark and a chargino [117,118].

We note in passing that interesting final state signatures can be obtained for the decays of bottom squarks as well [119]. For example $\tilde{b}_L$ decays to a bottom quark and the bino-like neutralino with a branching ratio close to 71% and $\tilde{b}_R$ decays to a top quark and an electron with a branching close to 47% in the first bench mark (BP-I) scenario. Such a branching would imply 2 b jets + $\not{E}_T$ or 2 b jets + 4 leptons + $\not{E}_T$ in the final states, respectively. The most stringent limit on the mass of the bottom squark comes from the search where it decays to a bottom quark and the lightest neutralino (LSP) with BR $(\tilde{b} \to b\tilde{\chi}_1^0) = 100\%$. Bottom squark mass up to 700 GeV has been excluded at 95% confidence level for neutralino mass less than 50 GeV [120]. We note that all the benchmark points are chosen in a way such that they satisfy existing bounds on top squark mass under various circumstances pertaining to its decay.

VI. THE BENCHMARKS AND THE FINAL STATES

In this section we discuss a few benchmark scenarios that would be broadly representative of the phenomenology that is expected of the framework under consideration. As mentioned earlier in Sec. III, we embed the model in SARAH (v4.4.1) [73–75]. We use the low energy output of SARAH (v4.4.1) and generate the SUSY spectrum using SPheno (v3.3.3) [121,122]. FlavorKit [123] is used to ensure benchmark points are consistent with all relevant flavor-violating constraints. Higgs boson cross sections and signal strengths are computed using HiggsBounds [124–127] and HiggsSignals [128,129]. As discussed earlier, we will mainly consider two regimes, viz., $\mu_u > m_{\tilde{t}_{1,2}}$ and $\mu_u < m_{\tilde{t}_{1,2}}$. For each case, we point out the dominant decay modes of both $\tilde{t}_1$ and $\tilde{t}_2$. These dictate the types of interesting signatures at the LHC for each of these cases.

A. Case 1: $\mu_u < m_{\tilde{t}_{1,2}}$

Two benchmark points for this case are shown in Table II. A relatively low value of $\mu_u (= 200$ GeV) is chosen for both the benchmark points. The masses of the Higgsino-like chargino and the neutralinos are mainly controlled by μ_u. We assume the singlet and the triplet VEVs to be small, roughly to be around 10^{-4} GeV. The

[4]Note however, that if $\tilde{t} \to b\tau^+$ opens up, the corresponding lower bound on the top squark mass can be relaxed. The decay $\tilde{t} \to b\tau^+$ is mostly controlled by the R-parity violating coupling λ'_{333}. The existing bound on this particular coupling is much relaxed: $\lambda'_{333} < 1.4 \cos\beta$ [45] and can be saturated for small values of $\tan\beta (\leq 5)$. However, in the present scenario we confine ourselves in the limit where $\tan\beta \gtrsim 20$, which renders the decay $\tilde{t} \to b\tau^+$ insignificant. On the other hand, the decay $\tilde{t} \to b\mu^+$ is also negligible because of the strong constraint $|\lambda'_{233}| < 6.8 \times 10^{-3} \cos\beta$ [100].

TABLE II. Benchmark sets of input parameters in the large neutrino Yukawa coupling (f) scenario and the resulting mass values for some relevant excitations for $\mu_u < m_{\tilde{t}_{1,2}}$ (case 1). M_3^D denotes the Dirac gluino mass. Also indicated are some of the relevant flavor observables and their values, all of which are currently allowed by experiments. The corresponding values of $\mu_{\gamma\gamma}$ (the estimated Higgs diphoton rate compared to its SM expectation) are also mentioned.

Parameters	BP-1	BP-2
M_1^D	1200 GeV	800 GeV
M_2^D	1200.1 GeV	800.1 GeV
M_3^D	1500 GeV	1500 GeV
μ_u	200 GeV	200 GeV
$m_{3/2}$	20 GeV	20 GeV
$\tan\beta$	23	35
$(m_u^2)_{33}$	2.3×10^5 GeV^2	2.5×10^5 GeV^2
$(m_Q^2)_{33}$	5.5×10^5 GeV^2	6.1×10^5 GeV^2
f	1	1
v_S	2×10^{-4} GeV	1.5×10^{-4} GeV
v_T	10^{-4} GeV	10^{-4} GeV
λ_S	1.130	1.116
$B\mu_L$	$-(200\text{ GeV})^2$	$-(200\text{ GeV})^2$
t_S	$(174\text{ GeV})^3$	$(174\text{ GeV})^3$
Observables	**BP-1**	**BP-2**
m_h	124.9 GeV	125.7 GeV
$m_{\tilde{t}_1}$	566.2 GeV	580.5 GeV
$m_{\tilde{t}_2}$	918.5 GeV	904.8 GeV
$m_{\tilde{\chi}_1^0} \equiv m_{\nu_e}$	0.01 eV	0.04 eV
$m_{\tilde{\chi}_2^0}$(bino-like)	167.9 MeV	168.3 MeV
$m_{\tilde{\chi}_3^0}$	211.5 GeV	213.8 GeV
$m_{\tilde{\chi}_4^0}$	211.5 GeV	213.8 GeV
$m_{\tilde{\chi}_1^+} \equiv m_e$	0.51 MeV	0.51 MeV
$m_{\tilde{\chi}_2^+}$	243.8 GeV	247.1 GeV
Flavor observables	**BP-1**	**BP-2**
BR$(B \to X_S\gamma)$	3.4×10^{-4}	3.3×10^{-4}
BR$(B_S^0 \to \mu\mu)$	2.4×10^{-9}	2.5×10^{-9}
BR$(\mu \to e\gamma)$	3.8×10^{-24}	4.9×10^{-24}
BR$(\mu \to 3e)$	3.0×10^{-26}	4.0×10^{-26}
$\mu_{\gamma\gamma}$	1.05	1.06

Dirac gluino mass (M_3^D) is considered to be 1.5 TeV. Since we are considering a small amount of R breaking, the Majorana gaugino masses are roughly around a few hundred MeV. Fixing the order parameter of R breaking, i.e., the gravitino mass $\mathcal{O}(10\text{ GeV})$, fixes these soft-SUSY breaking parameters. Both λ_S and λ_T are considered to be large, which for large $\tan\beta$ (>20), provide significant radiative corrections to the Higgs boson mass through one-loop quartic terms. Such a choice allows us to have a situation where both the top squarks are moderately light. Note that the chosen values of $m_{\tilde{t}_1}$(~470 GeV) for BP-1 and BP-2 are expected to be consistent with the latest LHC bounds discussed in Sec. V C. The bound assuming BR$(\tilde{t}_1 \to b\tilde{\chi}_1^+) = 100\%$ is evidently satisfied while the one ($m_{\tilde{t}_1} > 550$ GeV) that assumes BR$(\tilde{t}_1 \to t\tilde{\chi}_1^0) = 100\%$ is not applicable here (see Table III). Furthermore, the neutrino Yukawa coupling f is chosen to be 1. Hence, to have the active neutrino mass in the right ballpark, we need to consider the Dirac bino and wino masses to be almost degenerate. As conspicuous from Eq. (19), this degeneracy provides a suitable suppression to the neutrino Majorana mass when the Dirac gaugino masses themselves are roughly around a TeV or so. Some of the low energy flavor-violating branching ratios (which satisfy the respective experimental constraints) are also shown in Table II.

TABLE III. Decay branching fractions of $\tilde{t}_1$ in BP-1 and BP-2 for $\mu_u < m_{\tilde{t}_1}$.

Decay modes	BR for BP-1	BR for BP-2
$\tilde{t}_1 \to b\tilde{\chi}_2^+$	52.5%	51.7%
$\tilde{t}_1 \to t\tilde{\chi}_3^0$	20.0%	20.1%
$\tilde{t}_1 \to t\tilde{\chi}_4^0$	20.0%	20.1%
$\tilde{t}_1 \to t\tilde{\chi}_2^0$	6.0%	6.6%

1. Decay branching fractions of $\tilde{t}_1$

The dominant decay branching fractions of $\tilde{t}_1$ for BP-1 and BP-2 are indicated in Table III. $\tilde{\chi}_2^+$ is the Higgsino-like chargino and $\tilde{\chi}_{3,4}^0$ are the Higgsino-like neutralinos. $\tilde{\chi}_2^0$ is the bino-like neutralino with mass in the ballpark of a few hundred MeV. As can be seen from Table III, the top squarks, once produced in pairs, can undergo both symmetric as well as asymmetric decays. Table IV lists all possible final state topologies. However, in the context of this work, we will mainly consider the dilepton final states accompanied by b jets and MET. Such a final state might arise when the top squarks, on being pair produced, undergo the decay $\tilde{t}_1 \to b\tilde{\chi}_2^+$. $\tilde{\chi}_2^+$ in turn, decays to a W^+ and a $\tilde{\chi}_2^0(\tilde{\chi}_1^0)$ with a branching ratio close to 90% (10%) followed by W's decaying leptonically. Although a semileptonic ($\ell\nu jj$) final state from W decays is a good compromise between the rate and the cleanliness of the signal, we go for a cleaner channel where both the W bosons decay leptonically. As shown in Fig. 2(c), such a topology leads to a final state 2 b jets + 2 leptons + $\not{E}_T$. A similar final state could also arise from other decays of the lighter top squark, such as those involving $\tilde{t}_1 \to t\tilde{\chi}_2^0$ as shown in Figs. 2(a) and 2(b). However, the effective branching ratio is rather suppressed.

We note in passing that the various decay combinations shown in Table III could also provide exotic multilepton and multijet final states depending on the leptonic or hadronic decays of both $W^\pm$ or Z bosons. For example, decays such as $\tilde{t}_1 \to t\tilde{\chi}_{3/4}^0$ could give rise to a 2 b jets + 6 leptons + $\not{E}_T$ final state. Some relevant final states arising

TABLE IV. Possible final states arising out of various decay modes of $\tilde{t}_1$ when $\mu_u < m_{\tilde{t}_1}$.

$\mu_u < m_{\tilde{t}_1}$: decays of $\tilde{t}_1$
$pp \to \tilde{t}_1\tilde{t}_1^* \to \widehat{b\tilde{\chi}_2^+}\,\widehat{\bar{b}\tilde{\chi}_2^-} \to b\widehat{W^+\tilde{\chi}_2^0}\,\bar{b}\widehat{W^-\tilde{\chi}_2^0} \to 2b + 2W + \not{E}_T$
$pp \to \tilde{t}_1\tilde{t}_1^* \to t\widehat{\tilde{\chi}_2^0}\,\bar{t}\widehat{\tilde{\chi}_2^0} \to b\widehat{W^+\tilde{\chi}_2^0}\,\bar{b}\widehat{W^-\tilde{\chi}_2^0} \to 2b + 2W + \not{E}_T$
$pp \to \tilde{t}_1\tilde{t}_1^* \to b\widehat{\tilde{\chi}_2^+}\,\bar{t}\widehat{\tilde{\chi}_2^0} + \text{H.c.} \to b\widehat{W^+\tilde{\chi}_2^0}\,\bar{b}\widehat{W^-\tilde{\chi}_2^0} + \text{H.c.} \to 2b + 2W + \not{E}_T$
$pp \to \tilde{t}_1\tilde{t}_1^* \to t\widehat{\tilde{\chi}_{3/4}^0}\,\bar{t}\widehat{\tilde{\chi}_2^0} + \text{H.c.} \to b\widehat{W^+Z\tilde{\chi}_2^0}\,\bar{b}\widehat{W^-\tilde{\chi}_2^0} + \text{H.c.} \to 2b + 2W + Z + \not{E}_T$
$pp \to \tilde{t}_1\tilde{t}_1^* \to b\widehat{\tilde{\chi}_2^+}\,\bar{t}\widehat{\tilde{\chi}_{3/4}^0} + \text{H.c.} \to b\widehat{W^+\tilde{\chi}_2^0}\,\bar{b}\widehat{W^-Z\tilde{\chi}_2^0} + \text{H.c.} \to 2b + 2W + Z + \not{E}_T$
$pp \to \tilde{t}_1\tilde{t}_1^* \to t\widehat{\tilde{\chi}_{3/4}^0}\,\bar{t}\widehat{\tilde{\chi}_{3/4}^0} \to b\widehat{W^+Z\tilde{\chi}_2^0}\,\bar{b}\widehat{W^-Z\tilde{\chi}_2^0} \to 2b + 2W + 2Z + \not{E}_T$

from the decays of $\tilde{t}_1$ are tabulated in Table IV. The branching fractions in BP-1 and BP-2 are rather similar since we are dealing with similar top squark masses. Also, top Yukawa coupling is practically insensitive to larger values of $\tan\beta$, as considered in our study. This results in similar branching fractions in the $b\tilde{\chi}^+$ mode in BP-1 and BP-2. The dynamics of other decays are essentially controlled by the gauge couplings and therefore, they remain similar.

2. Decay branching fractions of $\tilde{t}_2$

The dominant decay branching fractions of $\tilde{t}_2$ for BP-1 and BP-2 are shown in Table V. The pattern can be justified following the discussion in Sec. V B. The branching fractions of $\tilde{t}_2$ to the three modes indicated are comparable. These lead to distinct final state signatures with appreciable strength. Possible final states arising from the decays of $\tilde{t}_2$ are listed in Table VI. The decay channels $\tilde{t}_2 \to \tilde{t}_1 Z(h)$ are

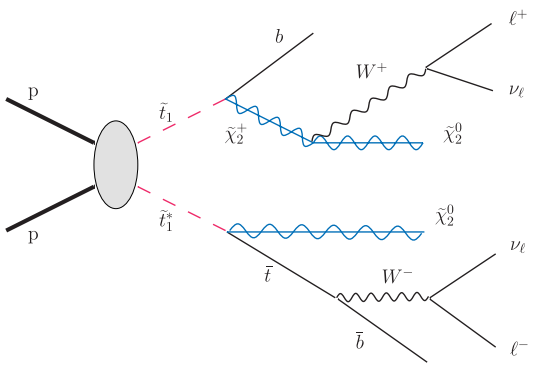

(a) Asymmetric decays of the top squarks with one decaying to $b\tilde{\chi}_2^+$ while the other decaying to $t\tilde{\chi}_2^0$, thus leading to $2b + 2\ell + \not{E}_T$ final state.

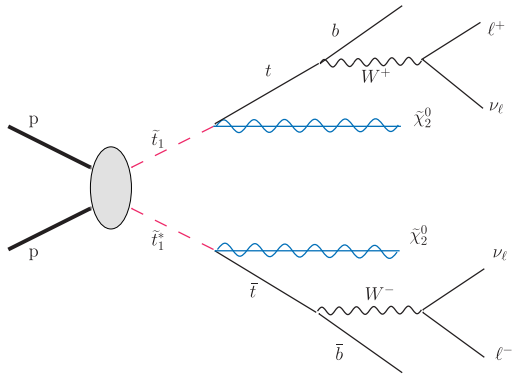

(b) Symmetric decays of top squarks with both decaying to $t\tilde{\chi}_2^0$, thus leading to $2b + 2\ell + \not{E}_T$ final state.

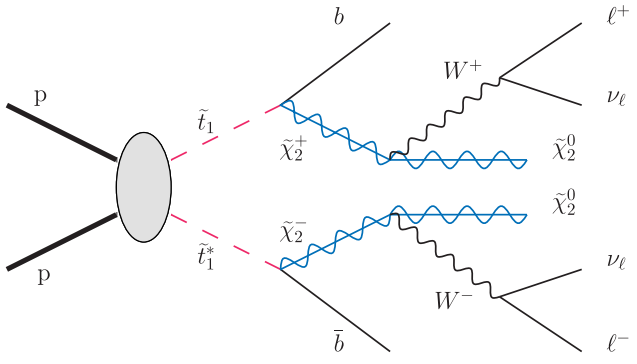

(c) Symmetric decays of top squarks with both decaying to $b\tilde{\chi}^\pm$, thus leading to $2b + 2\ell + \not{E}_T$ final state.

FIG. 2. The three figures described in (a), (b) and (c) correspond to final state topologies yielding $2b + 2\ell + E_T$ for case 1 scenario.

TABLE V. Decay branching fractions of $\tilde{t}_2$ in BP-1 and BP-2 for which $\mu_u < m_{\tilde{t}_2}$.

Decay modes	BR for BP-1	BR for BP-2
$\tilde{t}_2 \to be^+$	27.8%	47.2%
$\tilde{t}_2 \to t\tilde{\chi}_3^0$	35.7%	26.0%
$\tilde{t}_2 \to t\tilde{\chi}_4^0$	35.7%	26.0%

absent due to negligibly small mixing between the left- and the right-chiral states of the top squark. A remarkable point to note here is the significant decay branching fraction of $\tilde{t}_2$ to a bottom quark and an electron. To reiterate, this decay rate is proportional to λ'_{133}, which is identified with y_b. Therefore, the corresponding decay rate is large. Also, because of the large difference between the mass of the decaying particle ($\tilde{t}_2$) and the total mass of the particles in the final state ($m_b + m_e$), the final state electron is expected to be hard. The schematic diagram for such a process is presented in Fig. 3. Other decay modes presented in Table VI are similar to the previous case where the decay products of $\tilde{t}_2$ are a top quark and a Higgsino-like neutralino. These would further decay to give a final state comprised of 6 leptons + 2 b jets + $\not{E}_T$. The variations in the branching fractions as we go from BP-1 to BP-2, as can be seen in Table V, are due to changing bottom Yukawa coupling as $\tan\beta$ changes.

B. Case 2: $\mu_u > m_{\tilde{t}_{1,2}}$

As opposed to the previous case, we consider the situation where $\mu_u > m_{\tilde{t}_{1,2}}$. To have the Higgs boson mass in the right range we tweak λ_S. The soft masses $(m_u)^2_{33}$ and $(m_Q)^2_{33}$ are modified to get different top squark masses satisfying relevant LHC constraints. v_T just takes a different sign when compared to BP-1 and BP-2 only to exclude tachyonic states. All the other parameters are kept fixed to their values in Table II. Due to such a choice of μ_u, a top squark cannot decay to a Higgsino-like chargino and neutralinos. Note that, in the present case as well, the masses of the top squarks are chosen in such a manner that they satisfy the present experimental bounds. Values of flavor observables are checked to satisfy experimental constraints. However, those are not shown explicitly this time.

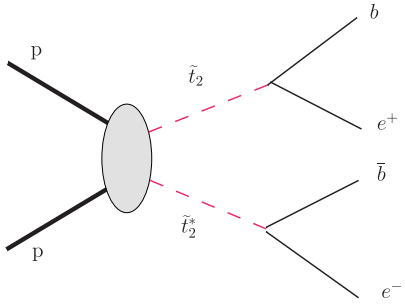

FIG. 3. $2b + e^+e^-$ final state arising from both $\tilde{t}_2$'s decaying directly to a bottom (antibottom) quark and a positron (electron).

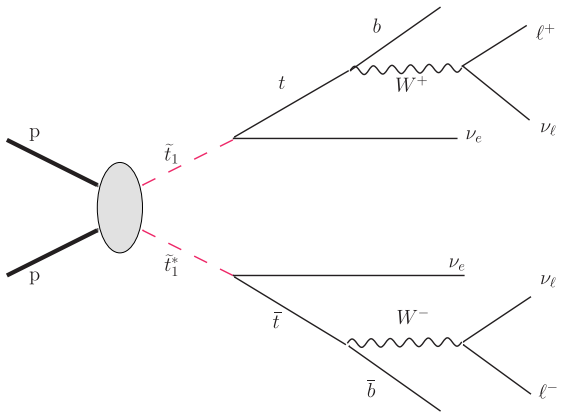

FIG. 4. Symmetric decays of $\tilde{t}_1$ and $\tilde{t}_1^*$ (via $t\nu_e$) mode leading to $2b + 2\ell + \not{E}_T$.

1. Decay branching fractions of $\tilde{t}_1$

The decay branching fractions for $\tilde{t}_1$ when $\mu_u > m_{\tilde{t}_{1,2}}$ are shown in Table VIII for the benchmark points BP-3 and BP-4. An interesting point to note here is that the top squark decays only to a top quark accompanied either by a $\tilde{\chi}_2^0$ [Fig. 2(b)] or a ν_e (Fig. 4) both of which are carriers of MET while the former being the dominant one. Again, both symmetric and asymmetric decays of the pair-produced $\tilde{t}_1$'s are possible. These would lead to 2 b-jets + $2\ell + \not{E}_T$ final states. Note that more exotic final states with a larger lepton multiplicity would be absent as heavier Higgsino-like neutralino(s) will now be missing in the cascades of $\tilde{t}_1$. This is in sharp contrast with what is expected for $\mu_u < m_{\tilde{t}_1}$

TABLE VI. Possible final states arising out of various decay modes of $\tilde{t}_2$ when $\mu_u < \tilde{m}_{t_2}$.

$\mu_u < m_{\tilde{t}_2}$: decays of $\tilde{t}_2$
$pp \to \tilde{t}_2\tilde{t}_2^* \to \widehat{be^+}\,\widehat{\bar{b}e^-} \to 2b + e^+e^-$
$pp \to \tilde{t}_2\tilde{t}_2^* \to \widehat{be^+}\,\bar{t}\widehat{\tilde{\chi}_{3/4}^0}$ +H.c. $\to \widehat{be^+}\,\bar{b}\widehat{W^-Z}\tilde{\chi}_2^0$ +H.c. $\to 2b + W + Z + e^+ + \not{E}_T$
$pp \to \tilde{t}_2\tilde{t}_2^* \to t\widehat{\tilde{\chi}_{3/4}^0}\,\bar{t}\widehat{\tilde{\chi}_{3/4}^0} \to b\widehat{W^+Z}\tilde{\chi}_2^0\,\bar{b}\widehat{W^-Z}\tilde{\chi}_2^0 \to 2b + 2W + 2Z + \not{E}_T$

TABLE VII. Same as in Table II but for an extra sign on v_T and for BP-3 and BP-4 for both of which $\mu_u > m_{\tilde{t}_{1,2}}$ (case 2). Values of flavor observables, not shown here explicitly, satisfy all the experimental constraints.

Parameters	BP-3	BP-4
μ_u	1500 GeV	1100 GeV
v_T	-10^{-4} GeV	-10^{-4} GeV
$(m_u^2)_{33}$	4×10^5 (GeV)^2	5×10^5 (GeV)^2
$(m_Q^2)_{33}$	5.2×10^5 (GeV)^2	6×10^5 (GeV)^2
λ_S	1.09	1.06
Observables	**BP-3**	**BP-4**
m_h	126.6 GeV	126.1 GeV
$m_{\tilde{t}_1}$	728.7 GeV	802.8 GeV
$m_{\tilde{t}_2}$	909.5 GeV	908.8 GeV
$m_{\tilde{\chi}_1^0} \equiv m_{\nu_e}$	0.03 eV	0.12 eV
$m_{\tilde{\chi}_2^0}$(bino-like)	175.8 MeV	175.6 MeV
$m_{\tilde{\chi}_3^0}$	1202.1 GeV	804.3 GeV
$m_{\tilde{\chi}_4^0}$	1202.2 GeV	804.3 GeV
$m_{\tilde{\chi}_1^+} \equiv m_e$	0.51 MeV	0.51 MeV
$m_{\tilde{\chi}_2^+}$	1304.2 GeV	877.4 GeV

TABLE VIII. Decay branching fractions of $\tilde{t}_1$ in BP-3 and BP-4 for which $\mu_u > m_{\tilde{t}_1}$.

Decay modes	BR for BP-3	BR for BP-4
$\tilde{t}_1 \to t\tilde{\chi}_2^0$	87.8%	94.6%
$\tilde{t}_1 \to t\nu_e$	12.2%	5.3%

TABLE IX. Decay branching fractions of $\tilde{t}_2$ for BP-3 and BP-4 for which $\mu_u > m_{\tilde{t}_2}$.

Decay modes	BR for BP-3	BR for BP-4
$\tilde{t}_2 \to be^+$	97.8%	98.7%
$\tilde{t}_2 \to t\tilde{\chi}_2^0$	1.8%	0.9%

(case 1) as discussed in Sec. VI A and thus, may be exploited to distinguish between these two broad scenarios.

2. Decay branching fractions of $\tilde{t}_2$

Similarly, the absence of a light Higgsino-like chargino and neutralinos implies $\tilde{t}_2$ would dominantly decay to a bottom quark and an electron (positron). The branching fractions of $\tilde{t}_2$ under such a circumstance are presented in Table IX.

VII. COLLIDER (LHC) ANALYSIS

In this section we present the setup and the results of the simulation we carry out at the 13 TeV LHC for pair-produced top squarks that eventually cascade to the final states discussed in Sec. VI.

A. The simulation setup and reconstructing the physics objects

We have implemented the model in MadGraph5_aMC@NLO [130]. Events for both signals and backgrounds are generated using the same. We use the parton distribution function CTEQ6L1 [131] and a factorization/renormalization scale of $\sqrt{m_{\tilde{t}_1} m_{\tilde{t}_2}}$ for generating events at the lowest order. The inclusive rates are then normalized to their respective values obtained after higher-order corrections as given by MadGraph5_aMC@NLO in the cases for the SM background and Prospino2 (v2.1) [132,133] for the case of the SUSY productions. Appropriate branching fractions are obtained from the spectrum generator SPheno [121] which, in the first place, is generated by SARAH [73–75]. We note in passing that the production cross section for the top squarks (at the tree level) in this model is same as in the MSSM, considering only the dominant strong interaction.

Events in the Les Houches (LHE) format are fed into Pythia 6.4.28 [134] for showering, hadronization and jet formation. Clustering of jets is performed with the built-in Pythia module PYCELL which employs a cone algorithm and incorporates appropriate smearing of the momenta. In PYCELL we allowed for an angular coverage of $|\eta| < 5$ for the hadron calorimeter with a cell segmentation of $\Delta\eta \times \Delta\phi = 0.1 \times 0.1$ which resembles a generic LHC detector. A cell is required to have a minimum value of deposited $E_T = 1$ GeV for it to be considered. A jet-cone radius of $\Delta R(j,j) = 0.4$ is employed for finding jets. A minimum summed E_T of 20 GeV is required within such a geometry for the configuration to be considered as a jet. Ultimately, formed jets within $|\eta| < 2.5$ are considered in our analysis. Care has been taken to isolate final state leptons by imposing the following cuts and isolation criteria:

(i) To select leptonic events we have used $p_T^\ell > 10$ GeV and $|\eta_\ell| < 2.4$.
(ii) Lepton-lepton separation has been done by choosing $\Delta R(\ell', \ell) > 0.2$, where $\Delta R = \sqrt{(\Delta\eta)^2 + (\Delta\phi)^2}$.
(iii) Subsequently, to separate leptons from jets we have used $\Delta R(j, \ell) > 0.5$.
(iv) Finally, the sum of the energy deposits of the hadrons which fall within a cone of $\Delta R \leq 0.2$ around a lepton, must be less than 10 GeV.

In this work, by leptons we mean only electrons and muons for which the detection efficiencies are generally very high, unlike the τ lepton. We have used a minimum p_T cut of 10 and 17 GeV to isolate muons and electrons, respectively. To estimate the number of b jets in the final state, a flat (but somewhat conservative) b-tagging efficiency of 60% has been used.

B. Top squark pair-production cross section

The phenomenology we discuss in this work crucially depends on the rate of pair production of the top squarks. It

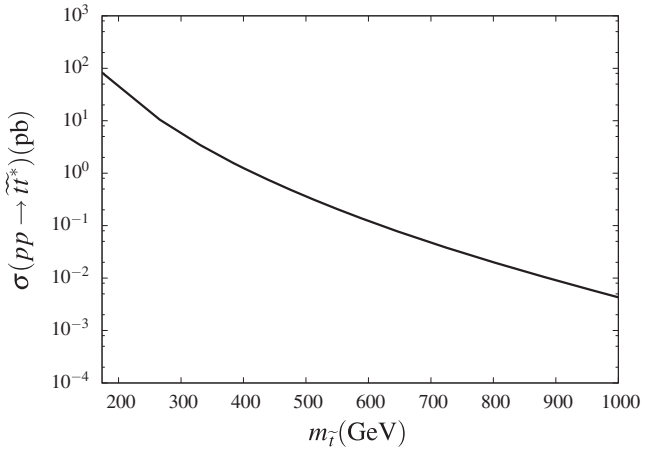

FIG. 5. Variation of production cross section for a pair of top squarks at the 13 TeV LHC. Other parameters are kept fixed at values given for BP-4 in Table VII (see text). Rates include appropriate K factors obtained from the package Prospino2.

is to be noted that at the lowest order these rates are the same as in the MSSM. Considering the dominant strong contributions in the rates, the variation of the same is only dependent on the mass of the top squark, irrespective of its chiral content. As a quick reckoner for this basic rate, we present the same as a function of $m_{\tilde{t}}$ in Fig. 5 for the 13 TeV run of the LHC. Appropriate K factors as obtained from the package Prospino2 [132,133] are already folded in. To this end, we fix all the parameters as given in BP-4 except for the right handed soft squark mass, which we varied from -4×10^4 GeV$^2 < (m_u^2)_{33} < 8 \times 10^5$ GeV^2. Such a choice would surely move the Higgs mass away from the allowed range. However, we are here merely concentrating on study of the production cross section for $\tilde{t}\tilde{t}^*$. The parameters such as λ_S, λ_T can be adjusted to fit the Higgs mass, which is unlikely to affect the production rate significantly (via unknown higher-order effects).

C. The Standard Model backgrounds

As mentioned earlier, we would mostly concentrate on the final states with 2 b jets + 2 leptons + $\not{E}_T$ and 2 b jets + e^+e^-. In the first case, we consider only the most dominant background coming from $t\bar{t}$ production when both the top quarks decay leptonically. In order to have a realistic normalization of this background, $t\bar{t}$ events generated at the lowest order (LO) using MadGraph5_aMC@NLO and the size of the event sample is scaled appropriately to correspond to its next-to-leading-order (NLO) + next-to-next-to-leading- log (NNLL) cross section (≈816 pb) [135]. The heavier top squark undergoes a significant decay to a bottom quark and an electron. The dominant background comes from the direct production of a pair of bottom quarks with one of them radiating a Z or γ^* which subsequently produces a pair of e^+e^-. This background can be largely suppressed by putting an on-shell Z veto for the e^+e^- pair. To be conservative and for the robustness of the estimate, the NLO computation [136–139] is done with two additional jets (10 GeV $< p_T^{\rm jet} <$ 60 GeV) in the final state. The SM cross section for $pp \to b\bar{b}e^+e^-$ + jets we used is 9.43 pb.

D. Event selection

To optimize the signal-to-background ratios, we now have to adopt a set of event selection criteria. Towards this, various appropriate kinematic distributions are studied for both signals and the backgrounds. We present our study for two broad scenarios discussed in Sec. VI, i.e., for $\mu_u < m_{\tilde{t}_{1,2}}$ and $\mu_u > m_{\tilde{t}_{1,2}}$. For each of these cases, two different final states are considered, viz., 2 b jets + 2 leptons + $\not{E}_T$ and $b\bar{b}e^+e^-$, arising from $\tilde{t}_1$ and $\tilde{t}_2$ decays, respectively.

1. Case 1: $\mu_u < m_{\tilde{t}_{1,2}}$

Here we discuss the decays of both the top squarks pertaining to the case where $\mu_u < m_{\tilde{t}_{1,2}}$.

$pp \to \tilde{t}_1\tilde{t}_1^* \to b\tilde{\chi}_2^+/t\tilde{\chi}_2^0 \to 2b\,\text{jets} + 2\,\text{leptons} + \not{E}_T$ *(Fig. 2).*— Such a final state could arise from top squarks decaying to $b\tilde{\chi}_2^\pm$ and/or $t\tilde{\chi}_2^0$. The final state leptons arise from the decays of W bosons. In addition, $\tilde{\chi}_2^\pm$ is somewhat heavier than the top quark for both BP-1 and BP-2. Hence, on an average, one would expect the leptons to be a little harder compared to the background leptons originating in the cascades of the top quarks. This can be seen from the left panel of Fig. 6, where the p_T distributions of the harder lepton in the signal in both the benchmarks have extended tails compared to a similar lepton originating from the SM background. The signal distributions for BP-1 and BP-2 are similar because of similar values of top squark masses in the two benchmarks. The signal $\not{E}_T$ distributions are different from the corresponding distribution for the SM background. This may be attributed to the much larger mass of the top squark (compared to m_t) and the presence of extra carriers of $\not{E}_T$, i.e., the bino-like MeV neutralino ($\tilde{\chi}_2^0$) and the active neutrino (ν_e) emerging from top squark decays. It is evident from the right panel of Fig. 6 that the SM background can be effectively suppressed by applying a hard enough $\not{E}_T$ cut, viz., $\not{E}_T > 200$ GeV. We have also constructed the dileptonic stransverse mass variable to see if the SM background can be suppressed further. The stransverse mass is a kinematic variable which is used to measure the masses of the pair-produced semi-invisibly decaying heavy particles. The dileptonic stransverse mass is defined as [140]

$$M_{T2}^{\ell\ell}(p_T^{\ell_1}, p_T^{\ell_2}, \not{p}_T) = \min_{\not{p}_T = \not{p}_T^1 + \not{p}_T^2}[\max\{M_T(p_T^{\ell_1}, \not{p}_T^1), M_T(p_T^{\ell_2}, \not{p}_T^2)\}], \quad (38)$$

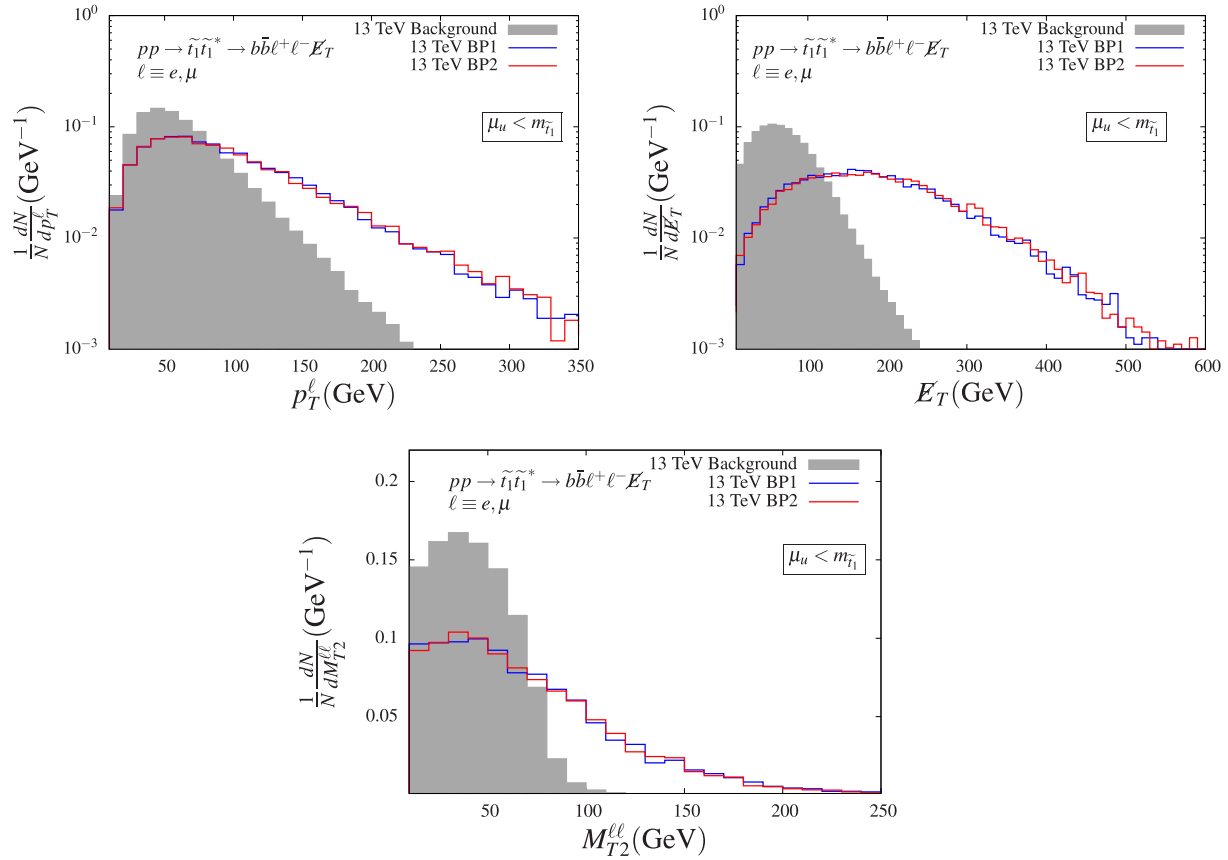

FIG. 6. p_T distributions of the harder lepton (left) and the $\not{E}_T$ distributions (right) for the background and the signals and dileptonic stransverse mass (in benchmark scenarios BP-1 and BP-2) in the 2 b jet + 2 lepton + $\not{E}_T$ final state arising from decays of $\tilde{t}_1$ for the case $\mu_u < m_{\tilde{t}_1}$.

where ℓ_1 and ℓ_2 are two isolated leptons and $\not{p}_T$ is the total missing transverse momentum in the event and the transverse mass of the system M_T has its usual definition. Although, the stransverse mass is a standard variable used in the recent top squark search, however, the yield with $\not{E}_T$ cut is more effective compared to the dileptonic $M_{T2}^{\ell\ell}$ cut for BP-1 and BP-2.

$pp \to \tilde{t}_2\tilde{t}_2^* \to b\bar{b}e^+e^-$ (Fig. 3).—As has been pointed out earlier, $\tilde{t}_2$ could have a significant decay branching fraction to a bottom quark and an electron, which is a characteristic of such a scenario. Along with the enlarged phase space available to this decay mode, a moderately large coupling ($\sim\lambda'_{133} \equiv y_b$) does boost the decay rate. Naturally, we expect electrons (positrons) with high p_T. In the absence of a genuine carrier of $\not{E}_T$ in such a final state, low or at most a moderate $\not{E}_T$ is expected from mismeasured momenta of the involved physics objects. The leptons are also expected to have uncorrelated momenta. Such events are rare in the SM. The left of panel Fig. 7 illustrates the hardest electron (positron) p_T distribution in the scenario where $\tilde{t}_2$ decays to a bottom quark and an electron (positron). We impose a minimum p_T cut of 200 GeV to reduce the SM background substantially. Since $m_{\tilde{t}_2}$ is very similar for BP-1 and BP-2 and so is its kinematics for these two benchmark points, the distributions look very similar. In the right panel of Fig. 7, we present the MET distribution which arises in this case from mismeasurements of momenta of visible entities in the final state. As expected, the MET distributions peak at small MET (≈25 GeV).

Note that eventually, one should be able to reconstruct $\tilde{t}_2$'s in the invariant mass spectra of appropriately chosen b-jet-electron (positron) systems which would show peaks at $m_{\tilde{t}_2}$. Clearly, the efficiency of reconstructing $\tilde{t}_2$ would be limited by various detector effects and a close study of the kinematic distributions discussed above would surely be of crucial help. Nonetheless, it appears that the peaks cannot be missed and a reasonable estimation of $m_{\tilde{t}_2}$ would thus be possible.

2. Case 2: $\mu_u > m_{\tilde{t}_{1,2}}$

For $\mu_u > m_{\tilde{t}_{1,2}}$, the top squarks decay mostly in a symmetric manner with $\tilde{t}_1 \to t\tilde{\chi}_2^0$ and $\tilde{t}_2 \to be^+$ as can be seen from Table IX.

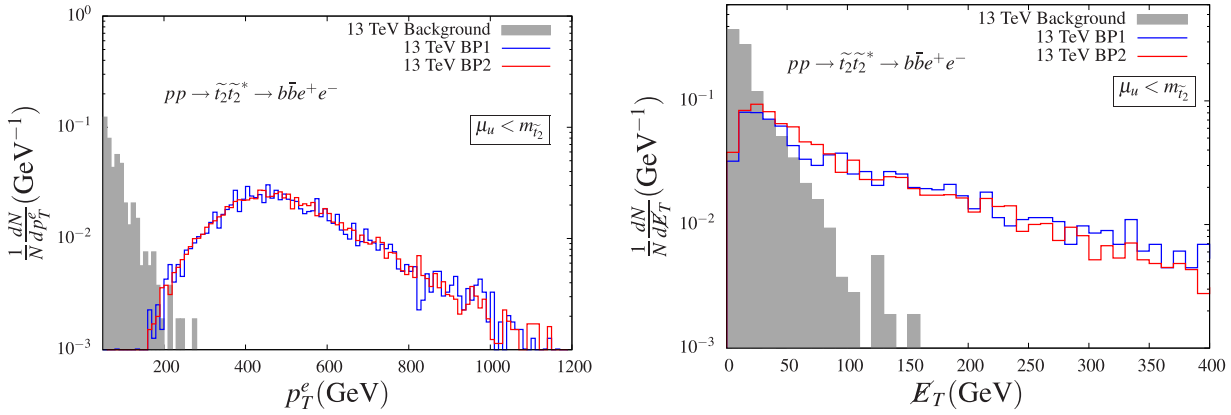

FIG. 7. p_T distributions of the harder electron (positron) from both background and signal (left) and $\not{E}_T$ distributions (right) (in benchmark scenarios BP-1 and BP-2) in the $b\bar{b}e^+e^-$ final state arising from decays of a pair of $\tilde{t}_2$'s for the case $\mu_u < m_{\tilde{t}_2}$.

$pp \to \tilde{t}_1\tilde{t}_1^* \to t\tilde{\chi}_2^0\bar{t}\tilde{\chi}_2^0 \to 2b\,\text{jets} + 2\text{leptons} + \not{E}_T$ *[Fig. 2(b)].*—For $\mu_u > m_{\tilde{t}_1}$, $\tilde{t}_1$ decays mostly to a top quark and a bino-like neutralino (see Table VIII). The top quark would subsequently decay to a W boson and a b jet via cascades. A pair of W's can then decay leptonically, semileptonically or hadronically. We confine ourselves to leptonic decays of W bosons for cleaner signals. The final state would then be comprised of $2\,b\,\text{jets} + 2\,\text{leptons} + \not{E}_T$. The p_T distributions for the harder of the final state leptons are shown in the left panel of Fig. 8. The presence of an additional source of $\not{E}_T$ and the heavier mass of $\tilde{t}_1$ in the signal are behind harder $\not{E}_T$ distributions (see right panel of Fig. 8) when compared to the SM background. To optimize the signal significance, we have observed the dileptonic $M_{T2}^{\ell\ell}$ cut of

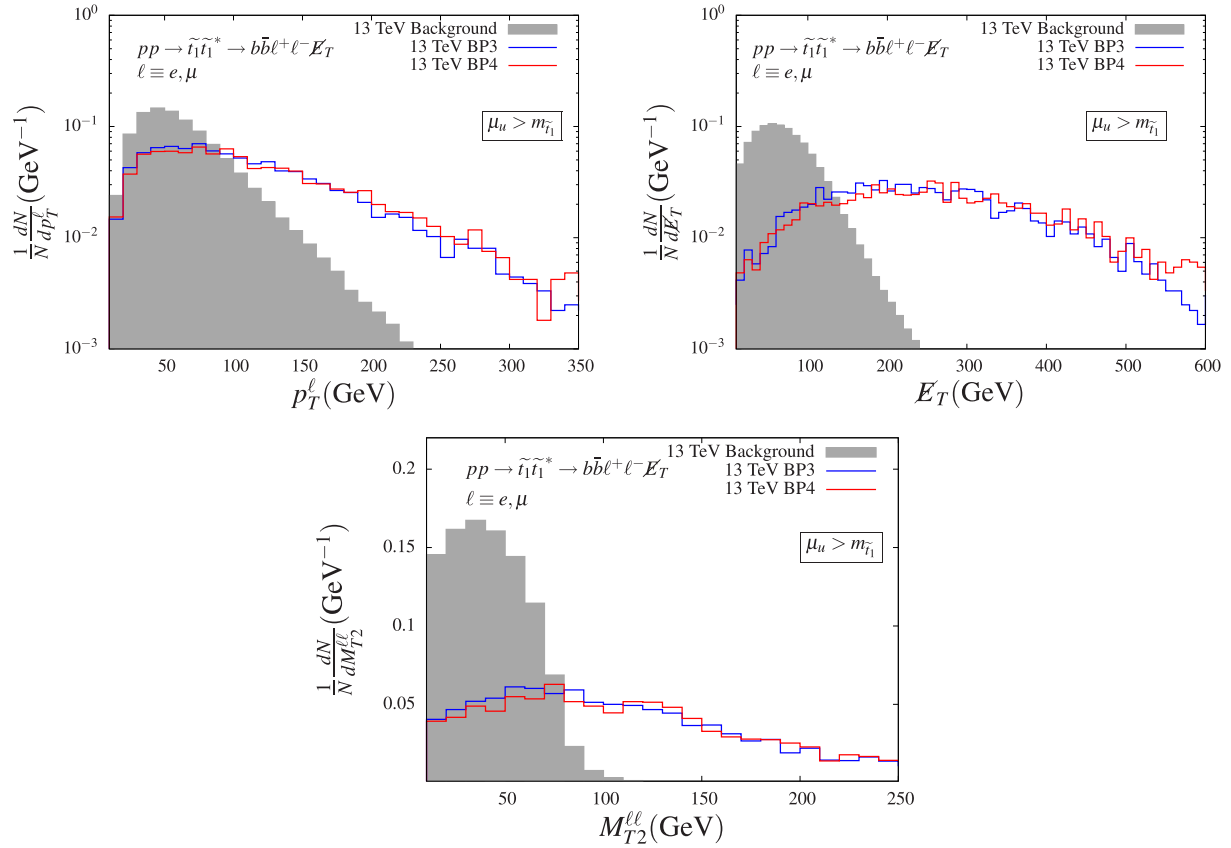

FIG. 8. p_T distributions of the harder lepton (left) and the $\not{E}_T$ distributions (right) and dileptonic stransverse mass for the background and the signals (in benchmark scenarios BP-3 and BP-4) in the $2\,b$ jet $+ 2$ lepton $+ \not{E}_T$ final state arising from decays of $\tilde{t}_1$ for the case $\mu_u > m_{\tilde{t}_1}$.

150 GeV works better compared to the $\not{E}_T$ cut of 200 GeV as used in case 1.

$pp \to \tilde{t}_2\tilde{t}_2^* \to b\bar{b}e^+e^-$ *(Fig. 3).*—In this case the overwhelmingly dominant decay mode is $\tilde{t}_2 \to be^+$. As mentioned earlier, the emitted electron (positron) could have a very high p_T as is evident from the left panel of Fig. 9. A strong p_T cut (> 200 GeV) on the electron can thus be easily afforded to suppress the SM background effectively. Similar to the case of Fig. 7, the distributions of MET (of spurious origin) for the present case are presented in the right panel of Fig. 9. Again, the MET distributions peak at small values ($\approx$25 GeV), as expected and explained earlier. Again, possible reconstructions of $\tilde{t}_2$'s in the invariant mass distributions of suitable pairs of b-jet-electron (positron) systems are on the cards. We will touch briefly on this issue later in this section.

It is also important to note that ATLAS has performed a search for RPV stops in this channel [141]. Our analysis strategy is somewhat different from what they have chosen. ATLAS uses a cut on hadronic transverse momentum $H_T > 1.1$ TeV and requires the invariant masses of the b-lepton pairs to be within 20% of each other. We find that the simple cut on electron momentum suppresses the background equally well and should be robust even at high pileup conditions.

Before going into the assessment of the signal significance, we mention below some issues of interest/importance pertaining to possible final states in these two cases.

(i) For both $\mu_u < m_{\tilde{t}_1}$ (Sec. VI A) and $\mu_u > m_{\tilde{t}_1}$ (Sec. VI B), we have only looked into the $2\,b$ jet + 2 lepton + $\not{E}_T$ final state arising from $\tilde{t}_1$ pair production. However, the first scenario is phenomenologically richer as it can yield multilepton signals with four to six leptons in the final states when $\tilde{t}_1$'s and $\tilde{t}_2$'s decay via cascades involving the heavier neutralinos and charginos that in turn decay to SM Z bosons (see Tables III and V). Some corroborative analyses can take advantage of such inclusive final states comprised of four to six leptons along with b jets and MET.

(ii) Furthermore, such a possibility could help differentiate $\tilde{t}_2$ from the two distinct scenarios considered in this work. For $\mu_u < m_{\tilde{t}_2}$, in addition to the $2\,b$ jets + e^+e^- final state out of which a pair of $\tilde{t}_2$'s could be reconstructed, there would also be multilepton final states where leptons other than $e^+(e^-)$ would appear. This is sharp contrast to the regime with $\mu_u > m_{\tilde{t}_2}$.

(iii) A final state like $2\,b$ jets + e^+e^- arising from the decays of $\tilde{t}_2$'s would be ideally free from any MET. However, as pointed out earlier, in reality, mismeasurements of various momenta may give rise to a low to moderate amount of MET thus rendering the final state arising from a pair of $\tilde{t}_2$'s to be similar to that obtained from $\tilde{t}_1$ pair production in a part of the phase space. This gives rise to some legitimate concern as to how efficiently the signature of $\tilde{t}_2$'s could be deciphered, given the rates for such a final state originating in $\tilde{t}_1$ pair production would be, in general, large thanks to smaller mass of $\tilde{t}_1$.

Such contaminations, however, can be avoided to a reasonable extent by imposing hard cuts on the minimum p_T of the leading electrons as guided by the lepton p_T distributions in the left panels of Figs. 6 and 7 (for $\mu_u < m_{\tilde{t}_1}$) and Figs. 8 and 9 (for $\mu_u > m_{\tilde{t}_1}$). In addition, imposition of a cut on the maximum allowed MET could effectively restrict the contamination thus allowing for a more efficient reconstruction of $\tilde{t}_2$. By studying the MET distributions presented in the right panels of Figs. 7 and 9, we find an optimal value of this cut to be $\not{E}_T < 50$ GeV that helps retain a healthy number of "signal" events with low $\not{E}_T$, a characteristic of such a final state originating in the decays of $\tilde{t}_2$.

In Fig. 10 we present the invariant mass distributions of appropriately chosen pairs of b jet and an

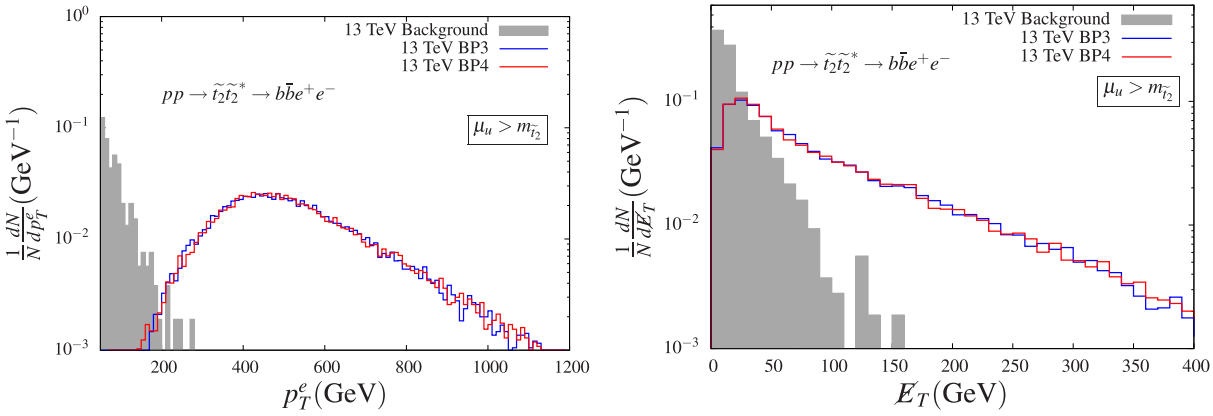

FIG. 9. Same as in Fig. 7 but for benchmark scenarios BP-3 and BP-4 and for the case $\mu_u > m_{\tilde{t}_2}$.

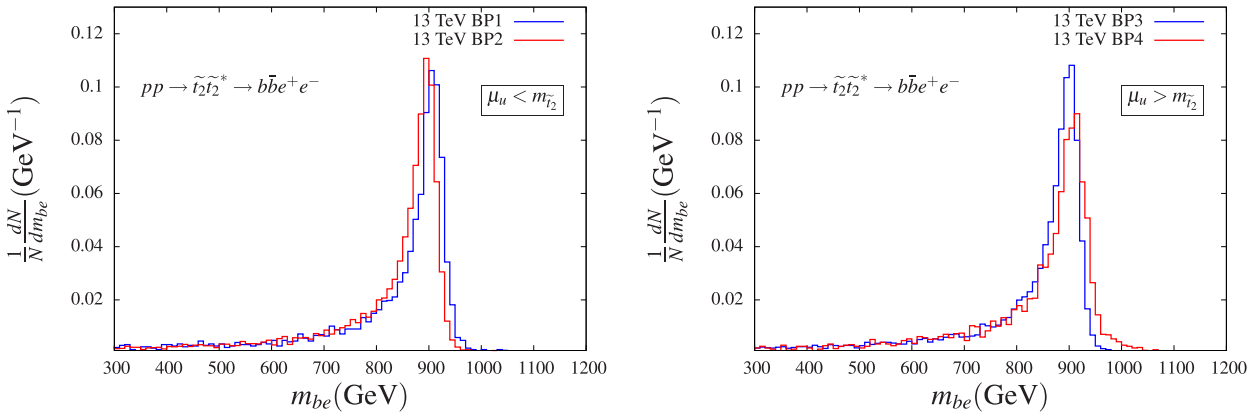

FIG. 10. Invariant mass distributions for the appropriate pairs of b-jet-electron (positron) systems [with low MET characteristic of R-parity violating decays of $\tilde{t}_2$ to a bottom quark and an electron (positron)] for $\mu_u < m_{\tilde{t}_2}$ (left) and $\mu_u > m_{\tilde{t}_2}$ (right). The distributions are obtained by imposing $p_T > 200$ GeV for the leading electron and $\not{E}_T < 50$ GeV.

electron (positron). Guided by Figs. 7 and 9, a high p_T threshold of 200 GeV for the leading electron is demanded along with requiring an $\not{E}_T < 50$ GeV to ensure that we mostly confine ourselves to the signal region. The left (right) panel of Fig. 10 represents the case with $\mu_u < m_{\tilde{t}_2}$ ($\mu_u > m_{\tilde{t}_2}$). We find that in both cases clear peaks at $m_{\tilde{t}_2}$ show up thus raising the hope that not only $\tilde{t}_2$-s could be discovered in this mode but also a reliable estimate of its mass would be possible.

Before we close this subsection we like to mention that although we have only discussed two broad scenarios, i.e., $\mu_u < m_{\tilde{t}_2}$ and $\mu_u > m_{\tilde{t}_2}$, other intermediate situations are all *a priori* viable. However, the expectations under those scenarios could be substantiated in a straightforward manner from the two cases we present. For example, an increase in value of μ_u from that in case 1 would result in suppression of the branching fractions to Higgsino-like neutralinos and charginos. With increasing μ_u, at some point, these decay modes (see Table III) would be closed for $\tilde{t}_1$ and $\text{BR}(\tilde{t}_1 \to t\tilde{\chi}_2^0) = 1$. At the same time, branching fractions to the Higgsino-like states for $\tilde{t}_2$ would also get suppressed before these decay modes get completely closed as it happens in case 2. A detailed study of possible correlations among the event rates in various final states could, in principle, shed light on the relative value of μ_u with respect to $m_{\tilde{t}_1}$ and $m_{\tilde{t}_2}$. However, this is beyond the scope of the present work.

E. Signal significance and the reach

The signal significance (σ) is estimated using the expression [142]

$$\sigma = \sqrt{2\left[(S+B)\ln\left(1+\frac{S}{B}\right) - S\right]} \tag{39}$$

which is appropriate for the situation with a small number of events (in particular when the number of background events is less than 50). Equation (39) is based on likelihood ratios and follows from the Poisson distribution. Here, S and B stand for the numbers of the signal and the background events, respectively after imposition of the set of optimal cuts discussed in Sec. VII D. The K factors for $\tilde{t}\tilde{t}^*$ are computed using Prospino2 (v2.1) [132,133].

We now estimate the required integrated luminosities for a 5σ reach of $\tilde{t}_1$ and $\tilde{t}_2$ in the four benchmark scenarios we consider. The final states we focus on are $2\,b$ jets + 2 leptons + $\not{E}_T$ and $b\bar{b}e^+e^-$, which stem from the decay of $\tilde{t}_1$ and $\tilde{t}_2$, respectively. For the first case (see Table X) the

TABLE X. Required values of integrated luminosities ($\mathcal{L}$) to obtain a 5σ significance in the final state at $\sqrt{s} = 13$ TeV. The most important SM background arising from $t\bar{t}$ pair production is normalized to a cross section of ≈816 pb obtained at the NLO + NNLL level (see Sec. VII C). The cut acceptance for the background is 2.3×10^{-4}. A flat b-tagging efficiency of 60% is used.

$pp \to \tilde{t}_1\tilde{t}_1^* \to 2b$ jets + 2leptons + $\not{E}_T$	BP-1	BP-2	BP-3	BP-4
$\sigma(pp \to \tilde{t}_1\tilde{t}_1^*)$ (fb)	428.9	463.4	193.0	73.6
Cut acceptance for signal ($E_T > 200$ GeV for BP-1 and BP-2) ($M_{T2}^{\ell\ell} > 150$ GeV for BP-3 and BP-4)	1.5×10^{-2}	1.6×10^{-2}	4.4×10^{-3}	4.4×10^{-3}
Required $\mathcal{L}(\text{fb}^{-1})$ for 5σ significance	256.0	316	2350.0	3000 (3σ)

TABLE XI. Required values of integrated luminosities ($\mathcal{L}$) to obtain a 5σ significance in the $2\,b$ jets $+ e^+e^-$ final state at $\sqrt{s} = 13$ TeV. The SM background (see Sec. VII C) at NLO is found to be 9.43 pb (see Sec. VII C). The cut acceptance for the background is 1.25×10^{-4}. A flat b-tagging efficiency of 60% is used.

$pp \to \tilde{t}_2\tilde{t}_2^* \to 2b$ jets $+ e^+e^-$	BP-1	BP-2	BP-3	BP-4
$\sigma(pp \to \tilde{t}_2\tilde{t}_2^*)$ (fb)	7.83	8.69	8.45	8.48
Cut acceptance for signal ($p_T > 200$ GeV, $\not{E}_T < 50$ GeV)	1.96×10^{-2}	5.26×10^{-2}	1.9×10^{-1}	1.9×10^{-1}
Required $\mathcal{L}(\text{fb}^{-1})$ for 5σ significance	501.23	63.92	6.85	6.61

dominant background comes from $t\bar{t}$ pair production which subsequently decays to the $2\,b\,\text{jet} + 2\,\text{lepton} + \not{E}_T$ final state. An appropriate K factor of ≈ 1.6 is used to derive the NLO cross sections from the LO ones for $\tilde{t}$-pair production.

We note that a 5σ signal significance can be achieved for BP-1 and BP-2, with an integrated luminosity around 100 fb^{-1}. To achieve a similar significance for BP-3 and BP-4, one has to wait for a much higher accumulated luminosity, for example, 500 and 3000 fb^{-1}, respectively at $\sqrt{s} = 13$ TeV.

In Table XI we present the required luminosities for a 5σ reach of $\tilde{t}_2$ for the four benchmark points. The dominant SM background comes from $b\bar{b}Z/\gamma^*$ production followed by Z/γ^* giving rise to e^+e^- pairs. This can be efficiently suppressed by using an on-shell Z veto for the e^+e^- pairs, as discussed in Sec. VII C. Thus, as can be seen from this table, a 5σ significance can be obtained with an integrated luminosity as low as <10 fb^{-1} for the benchmark scenarios BP-3 and BP-4 with $\sqrt{s} = 13$ TeV. In addition, we also study the H_T distribution, i.e., the scalar sum of the p_T of the e^+e^- pair and the reconstructed b jets and the improvements are marginal. The wildly varying integrated luminosities across the benchmark points are the artifact of varying branching fractions that are instrumental, as has been pointed out in Sec. VI.

Figure 11 summarizes the mass reach for the two top squarks with varying accumulated integrated luminosities (or, in other words, luminosity required to probe a certain top squark mass) at the 13 TeV LHC. The left panel illustrates the case for $\tilde{t}_1$ in the final state $2b + 2\,\text{lepton} + \not{E}_T$ in BP-2 while the right one does the same for $\tilde{t}_2$ via $2b + e^+e^-$ final state in BP-4. As indicated by Tables X and XI, Fig. 11 also reveals that $\tilde{t}_2$ has a significantly better reach compared to $\tilde{t}_1$ with the final states under consideration. This may lead to a tantalizing possibility of discovering $\tilde{t}_2$ of such a scenario much earlier than $\tilde{t}_1$ and the former could guide us to find the latter. We observe that at the 13 TeV LHC and with the mass reaches for $\tilde{t}_1$ and $\tilde{t}_2$ are around 575 (750) GeV and 1.2 (1.4) TeV respectively, with an integrated luminosity of 300 (3000) fb^{-1}.

VIII. THE STEALTH TOP SQUARK SCENARIO

The SUSY model under consideration, with superlight carriers of MET like $\tilde{\chi}_1^0 \equiv \nu_e$ and a MeV neutralino LSP ($\tilde{\chi}_2^0$) can easily conceive a rather low mass top squark lying right in the so-called stealth window of 197 GeV $\lesssim m_{\tilde{t}_1} \lesssim 205$ GeV [78]. As discussed in Sec. V C, the experimental lower bound on $m_{\tilde{t}_L}$ is more stringent considering its decay modes. Hence we choose $\tilde{t}_R$ to be the lightest top squark ($\tilde{t}_1$). A benchmark

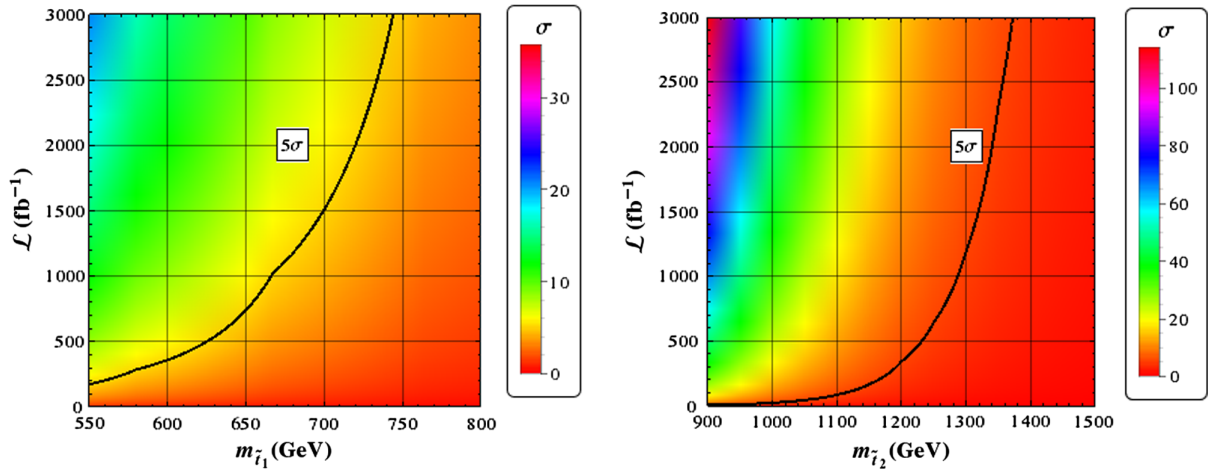

FIG. 11. Density plot reflecting the reach for top squark masses via $2\,b\,\text{jet} + 2\,\text{lepton} + \not{E}_T$ final state in BP-2 in the $m_{\tilde{t}_1} - \mathcal{L}$ plane (left) and via $2\,b\,\text{jet} + e^+e^-$ final state in BP-4 in the $m_{\tilde{t}_2} - \mathcal{L}$ plane (right). The thick black curves are contours of 5σ significance above and on the left of which the masses can be explored with $\geq 5\sigma$ significance. The cuts are kept fixed at values mentioned in the text for the respective cases.

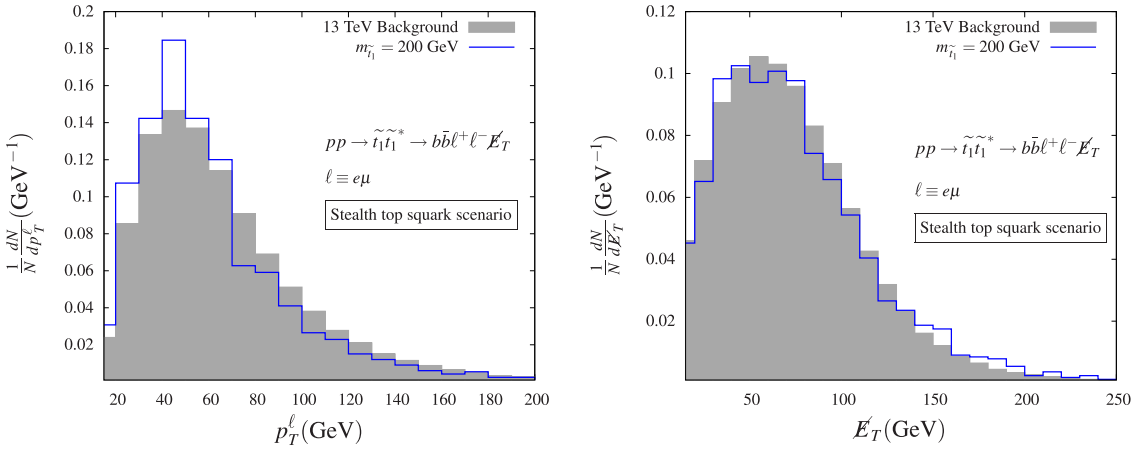

FIG. 12. p_T distributions of the harder lepton (left) and the $\not{E}_T$ distributions (right) for the background and the signal in the $2\,b\,\text{jet} + 2\,\text{lepton} + \not{E}_T$ final state arising from the decays of a pair of $\tilde{t}_1$'s in the stealth top squark scenario.

point can be obtained by choosing $(m_u^2)_{33} = -2.5 \times 10^4\,\text{GeV}^2$. This results in $m_{\tilde{t}_1} \sim 200\,\text{GeV}$. Such a light top squark cannot provide enough correction to the Higgs mass. Hence we choose a relatively large value of λ_S $(= 1.28)$ so that the radiatively generated additional quartic contributions could lift the Higgs boson mass to the observed range. All other parameters are fixed at the values mentioned in BP-1 (see Table II). Note that the additional tree level contribution proportional to the neutrino Yukawa coupling f remains small (even for its order one value) because of large values of $\tan\beta$ that we require. As a result, $\tilde{t}_1$ mostly decays to $t\tilde{\chi}_2^0$ and $\tilde{t}_1 \to t\nu_e$ with ∼85% and ∼15% branching fractions, respectively. The possible final state topologies are exactly the same as those that result from top quark pair production.

We again analyze the final state with $2b$jets$+$ 2leptons$+\not{E}_T$. We checked that the distributions of various kinematic observables look very similar for the signal and the $t\bar{t}$ background, which is something literally expected of a stealth top squark and what makes it so elusive. In Fig. 12 we present the p_T distribution of the harder lepton (left panel) and the $\not{E}_T$ distribution (right panel) which clearly demonstrate how similar the behaviors of the SM background and the signal could get. In this context, techniques to exploit differences in spin correlations inherent to $t\bar{t}$ and $\tilde{t}\tilde{t}^*$ systems [82], use of various transverse mass variables [143] including the one like m_{T_2} in the dileptonic decay channel [144], incorporating a new variable like "topness" [145] using asymmetric decays of the top squarks have been proposed to study the stealth top squark regime in search for an improved sensitivity. Clearly the issue demands dedicated addressal which is beyond the scope of the present discussion.

IX. SUMMARY AND CONCLUSIONS

We study a $U(1)_R$ lepton number model augmented with a right handed neutrino superfield. The R charges are identified with the lepton numbers in such a way that the sneutrinos acquire large VEVs. Such large VEVs for sneutrinos are not prohibited since, in such a scenario, the same are not constrained by the Majorana masses of the neutrinos. In this paper, we choose to work in a basis in which only the electron-type sneutrino acquires a nonzero VEV whereas the VEVs of the other two sneutrinos are rotated away. This simple extension with a right handed neutrino superfield is rather interesting in the sense that the Higgs boson mass gets a tree level contribution which can be substantial in the low $\tan\beta$ regime and for order one neutrino Yukawa coupling f. Also present is the large one-loop contribution to the Higgs boson mass arising from new couplings in the theory. Thus, one can easily accommodate a scenario where both top squarks are light. In addition, a very light bino-like neutralino comes out naturally in this scenario along with an active neutrino endowed with an appropriately small Majorana mass. Therefore, rich and interesting collider signatures are expected in such a scenario. The signature of a top squark decaying to a top quark and a neutralino and/or a neutrino is similar to the top quark pair production in the SM. Under favorable circumstances, a top squark could also decay to a bottom quark and a chargino leading to a similar final state containing two b jets and two leptons along with MET. In this mode, top squark mass of around 575 (750) GeV can be probed with 300 (3000) fb^{-1} of integrated luminosity.

Furthermore, in an R-parity violating scenario such as ours, the charginos mix with the electron. The decay width of the top squark to a bottom quark and an electron (positron) is enhanced because of the enhanced coupling λ'_{133} as well as an unsuppressed phase space. Hence we study in detail the final state with two b jets accompanied by an e^+e^- pair arising from such a dominant decay. We show that even when the top squark is heavy $[m_{\tilde{t}_2} \lesssim 1.2(1.4)\ \text{TeV}]$, this particular channel could deliver a large signal significance with 300 (3000) fb^{-1} of integrated luminosity.

In the model discussed in this work, only $\tilde{t}_2(\approx\tilde{t}_L)$ decays to be^+. This is an artifact of no $L-R$ mixing in the top squark sector. Also, note that the scenario prohibits $\tilde{t}_2$ decaying to $b\mu^+$ or $b\tau^+$. The final state arising from both top squarks decaying to the $be^+(\bar{b}e^-)$ mode could carry MET which can only be of spurious origin (mismeasurements of various visible momenta, defects in the detector, etc.) and hence is characteristically small. This feature can be used to establish such a model and differentiate it from other competing ones. Due to a relatively clean final state and hence, a possibility to reconstruct the heavier top squark mass reasonably efficiently, such a state could be within an easier reach of the current LHC run when compared to its lighter peer. Such a scenario thus, gives rise to an interesting possibility that $\tilde{t}_2$ can be found much earlier than $\tilde{t}_1$ at the LHC and could carry a reliable hint as to where exactly to look for the latter. The signal region for $\tilde{t}_1$ is attributed with a much larger MET as is usual in searches for new heavy states in scenarios with a stable charge- and color-neutral particle(s). This is in sharp contrast with the case of $\tilde{t}_2$ in such a scenario.

Although the analyses in this work are presented in terms of two broad scenarios, viz., $\mu_u < m_{\tilde{t}_2}$ and $\mu_u > m_{\tilde{t}_2}$, it is pointed out that the signatures discussed are robust under intermediate situations except for some obvious quantitative issues getting in. Simultaneous searches in various channels described in this work are expected to shed light on the detailed aspect of the spectrum and the involved new couplings of such a scenario.

Finally, we demonstrate how the stealth top squark can appear in our model naturally. However, probing such a window, 197 GeV $\lesssim m_{\tilde{t}} \lesssim$ 205 GeV [78] needs dedicated analysis which is an active area of research on its own merit. Overall, characteristic signatures for these light top squark states at the LHC even have the potential to discriminate between competing scenarios that may give rise to such a light pair of top squarks. In addition, such issues and projections are not readily available for the 13/14 TeV run. Therefore, it is important to study all these issues at the dawn of 13 TeV run of the LHC.

ACKNOWLEDGMENTS

S. C. would like to thank the Council of Scientific and Industrial Research, Government of India for the financial support received as a senior research fellow. It is a pleasure to thank Florian Staub for many helpful discussions regarding SARAH. S. C. would also like to thank Subhadeep Mondal, Arghya Choudhury and Amit Chakraborty for many helpful discussions. A. D. would like to thank the Department of Theoretical Physics, IACS for hospitality during the course of this work. S. R. acknowledges the hospitality of the University of Helsinki and Helsinki Institute of Physics where this work was initiated. K. H. and H. W. acknowledge support from the Academy of Finland (Project No. 137960).

[1] G. Aad *et al.* (ATLAS Collaboration), Phys. Lett. B **716**, 1 (2012).
[2] S. Chatrchyan *et al.* (CMS Collaboration), Phys. Lett. B **716**, 30 (2012).
[3] S. Chatrchyan *et al.* (CMS Collaboration), Eur. Phys. J. C **73**, 2568 (2013).
[4] G. Aad *et al.* (ATLAS Collaboration), J. High Energy Phys. 10 (2013) 130; 01 (2014) 109(E).
[5] G. Aad *et al.* (ATLAS Collaboration), J. High Energy Phys. 09 (2014) 176.
[6] P. Fayet, Phys. Lett. **64B**, 159 (1976).
[7] J. Polchinski and L. Susskind, Phys. Rev. D **26**, 3661 (1982).
[8] L. J. Hall, Mod. Phys. Lett. A **05**, 467 (1990).
[9] L. J. Hall and L. Randall, Nucl. Phys. **B352**, 289 (1991).
[10] I. Jack and D. R. T. Jones, Phys. Lett. B **457**, 101 (1999).
[11] P. J. Fox, A. E. Nelson, and N. Weiner, J. High Energy Phys. 08 (2002) 035.
[12] A. E. Nelson, N. Rius, V. Sanz, and M. Unsal, J. High Energy Phys. 08 (2002) 039.
[13] Z. Chacko, P. J. Fox, and H. Murayama, Nucl. Phys. **B706**, 53 (2005).
[14] I. Antoniadis, K. Benakli, A. Delgado, M. Quiros, and M. Tuckmantel, Phys. Lett. B **634**, 302 (2006).
[15] I. Antoniadis, K. Benakli, A. Delgado, M. Quiros, and M. Tuckmantel, Nucl. Phys. **B744**, 156 (2006).
[16] I. Antoniadis, K. Benakli, A. Delgado, and M. Quiros, Adv. Studies Theor. Phys. **2**, 645 (2008).
[17] G. D. Kribs, E. Poppitz, and N. Weiner, Phys. Rev. D **78**, 055010 (2008).
[18] S. Y. Choi, M. Drees, A. Freitas, and P. M. Zerwas, Phys. Rev. D **78**, 095007 (2008).
[19] S. D. L. Amigo, A. E. Blechman, P. J. Fox, and E. Poppitz, J. High Energy Phys. 01 (2009) 018.
[20] K. Benakli and M. D. Goodsell, Nucl. Phys. **B816**, 185 (2009).
[21] A. E. Blechman, Mod. Phys. Lett. A **24**, 633 (2009).
[22] G. Belanger, K. Benakli, M. Goodsell, C. Moura, and A. Pukhov, J. Cosmol. Astropart. Phys. 08 (2009) 027.
[23] K. Benakli and M. D. Goodsell, Nucl. Phys. **B830**, 315 (2010).
[24] A. Kumar, D. Tucker-Smith, and N. Weiner, J. High Energy Phys. 09 (2010) 111.
[25] B. A. Dobrescu and P. J. Fox, Eur. Phys. J. C **70**, 263 (2010).

[26] K. Benakli and M. D. Goodsell, Nucl. Phys. **B840**, 1 (2010).
[27] S. Y. Choi, D. Choudhury, A. Freitas, J. Kalinowski, J. M. Kim, and P. M. Zerwas, J. High Energy Phys. 08 (2010) 025.
[28] L. M. Carpenter, J. High Energy Phys. 09 (2012) 102.
[29] G. D. Kribs, T. Okui, and T. S. Roy, Phys. Rev. D **82**, 115010 (2010).
[30] S. Abel and M. Goodsell, J. High Energy Phys. 06 (2011) 064.
[31] K. Benakli, M. D. Goodsell, and A.-K. Maier, Nucl. Phys. **B851**, 445 (2011).
[32] J. Kalinowski, Acta Phys. Pol. B **42**, 2425 (2011).
[33] K. Benakli, Fortschr. Phys. **59**, 1079 (2011).
[34] C. Frugiuele and T. Gregoire, Phys. Rev. D **85**, 015016 (2012).
[35] H. Itoyama and N. Maru, Int. J. Mod. Phys. A **27**, 1250159 (2012).
[36] C. Brust, A. Katz, S. Lawrence, and R. Sundrum, J. High Energy Phys. 03 (2012) 103.
[37] K. Rehermann and C. M. Wells, arXiv:1111.0008.
[38] R. Davies and M. McCullough, Phys. Rev. D **86**, 025014 (2012).
[39] E. Bertuzzo and C. Frugiuele, J. High Energy Phys. 05 (2012) 100.
[40] R. Davies, J. High Energy Phys. 10 (2012) 010.
[41] R. Argurio, M. Bertolini, L. Di Pietro, F. Porri, and D. Redigolo, J. High Energy Phys. 08 (2012) 086.
[42] M. D. Goodsell, J. High Energy Phys. 01 (2013) 066.
[43] R. Fok, G. D. Kribs, A. Martin, and Y. Tsai, Phys. Rev. D **87**, 055018 (2013).
[44] R. Argurio, M. Bertolini, L. Di Pietro, F. Porri, and D. Redigolo, J. High Energy Phys. 10 (2012) 179.
[45] C. Frugiuele, T. Gregoire, P. Kumar, and E. Ponton, J. High Energy Phys. 03 (2013) 156.
[46] C. Frugiuele, T. Gregoire, P. Kumar, and E. Ponton, J. High Energy Phys. 05 (2013) 012.
[47] K. Benakli, M. D. Goodsell, and F. Staub, J. High Energy Phys. 06 (2013) 073.
[48] F. Riva, C. Biggio, and A. Pomarol, J. High Energy Phys. 02 (2013) 081.
[49] H. Itoyama and N. Maru, Phys. Rev. D **88**, 025012 (2013).
[50] H. Itoyama and N. Maru, Symmetry **7**, 193 (2015).
[51] P. Agrawal and C. Frugiuele, J. High Energy Phys. 01 (2014) 115.
[52] S. Chakraborty and S. Roy, J. High Energy Phys. 01 (2014) 101.
[53] C. Csaki, J. Goodman, R. Pavesi, and Y. Shirman, Phys. Rev. D **89**, 055005 (2014).
[54] E. Dudas, M. Goodsell, L. Heurtier, and P. Tziveloglou, Nucl. Phys. **B884**, 632 (2014).
[55] H. Beauchesne and T. Gregoire, J. High Energy Phys. 05 (2014) 051.
[56] E. Bertuzzo, C. Frugiuele, T. Gregoire, and E. Ponton, J. High Energy Phys. 04 (2015) 089.
[57] K. Benakli, M. Goodsell, F. Staub, and W. Porod, Phys. Rev. D **90**, 045017 (2014).
[58] S. Chakraborty, D. K. Ghosh, and S. Roy, J. High Energy Phys. 10 (2014) 146.
[59] M. D. Goodsell and P. Tziveloglou, Nucl. Phys. **B889**, 650 (2014).
[60] S. Ipek, D. McKeen, and A. E. Nelson, Phys. Rev. D **90**, 076005 (2014).
[61] D. Busbridge, arXiv:1408.4605.
[62] P. Dießner, J. Kalinowski, W. Kotlarski, and D. Stöckinger, J. High Energy Phys. 12 (2014) 124.
[63] S. Chakraborty, A. Datta, and S. Roy, J. High Energy Phys. 02 (2014) 124; 09 (2015) 077.
[64] A. E. Nelson and T. S. Roy, Phys. Rev. Lett. **114**, 201802 (2015).
[65] S. P. Martin, Phys. Rev. D **92**, 035004 (2015).
[66] J. Berger, J. A. Dror, and W. H. Ng, J. High Energy Phys. 09 (2015) 156.
[67] M. D. Goodsell, M. E. Krauss, T. Müller, W. Porod, and F. Staub, J. High Energy Phys. 10 (2015) 132.
[68] T. Schwetz, M. Tortola, and J. W. F. Valle, New J. Phys. **13**, 063004 (2011).
[69] T. Schwetz, M. Tortola, and J. W. F. Valle, New J. Phys. **13**, 109401 (2011).
[70] D. V. Forero, M. Tortola, and J. W. F. Valle, Phys. Rev. D **86**, 073012 (2012).
[71] M. C. Gonzalez-Garcia, M. Maltoni, J. Salvado, and T. Schwetz, J. High Energy Phys. 12 (2012) 123.
[72] W. Porod, M. Hirsch, J. Romao, and J. W. F. Valle, Phys. Rev. D **63**, 115004 (2001).
[73] F. Staub, arXiv:0806.0538.
[74] F. Staub, Comput. Phys. Commun. **184**, 1792 (2013).
[75] F. Staub, Adv. High Energy Phys. **2015**, 840780 (2015).
[76] D. Curtin, P. Meade, and P. J. Tien, Phys. Rev. D **90**, 115012 (2014).
[77] J. Beuria, A. Chatterjee, A. Datta, and S. K. Rai, J. High Energy Phys. 09 (2015) 073.
[78] G. Aad *et al.* (ATLAS Collaboration), Eur. Phys. J. C **75**, 510 (2015).
[79] J. Fan, M. Reece, and J. T. Ruderman, J. High Energy Phys. 11 (2011) 012.
[80] C. Csaki, L. Randall, and J. Terning, Phys. Rev. D **86**, 075009 (2012).
[81] J. Fan, M. Reece, and J. T. Ruderman, J. High Energy Phys. 07 (2012) 196.
[82] Z. Han and A. Katz, arXiv:1310.0356.
[83] M. Czakon, A. Mitov, M. Papucci, J. T. Ruderman, and A. Weiler, Phys. Rev. Lett. **113**, 201803 (2014).
[84] T. Eifert and B. Nachman, Phys. Lett. B **743**, 218 (2015).
[85] S. Chakraborty, Asesh Krishna Datta, Katri Huitu, Sourov Roy, and Harri Waltari (to be published).
[86] H. K. Dreiner, M. Hanussek, J. S. Kim, and S. Sarkar, Phys. Rev. D **85**, 065027 (2012).
[87] ATLAS Collaboration, Reports No. ATLAS-CONF-2013-037 and ATLAS-COM-CONF-2013-038, 2013.
[88] CMS Collaboration, Report No. CMS-PAS-SUS-12-023, 2012.
[89] ATLAS Collaboration, Reports No. ATLAS-CONF-2013-061 and ATLAS-COM-CONF-2013-071, 2013.
[90] S. Chatrchyan *et al.* (CMS Collaboration), Eur. Phys. J. C **73**, 2677 (2013).
[91] ATLAS Collaboration, Reports No. ATLAS-CONF-2015-015 and ATLAS-COM-CONF-2015-017, 2015.

[92] V. Khachatryan *et al.* (CMS Collaboration), Phys. Lett. B **739**, 229 (2014).
[93] R. Barbier, C. Berat, M. Besancon, M. Chemtob, A. Deandrea, E. Dudas, P. Fayet, S. Lavignac *et al.*, Phys. Rep. **420**, 1 (2005).
[94] S. Ambrosanio, G. L. Kane, G. D. Kribs, S. P. Martin, and S. Mrenna, Phys. Rev. D **54**, 5395 (1996).
[95] J. F. Gunion and H. E. Haber, Nucl. Phys. **B272**, 1 (1986); **B402**, 567(E) (1993).
[96] I. Low, Phys. Rev. D **88**, 095018 (2013).
[97] G. Aad *et al.* (ATLAS Collaboration), Phys. Rev. Lett. **114**, 142001 (2015).
[98] G. Aad *et al.* (ATLAS Collaboration), J. High Energy Phys. 06 (2014) 124.
[99] V. Khachatryan *et al.* (CMS Collaboration), Phys. Lett. B **739**, 229 (2014).
[100] H. K. Dreiner, K. Nickel, F. Staub, and A. Vicente, Phys. Rev. D **86**, 015003 (2012).
[101] A. Datta and B. Mukhopadhyaya, Phys. Rev. Lett. **85**, 248 (2000).
[102] S. P. Das, A. Datta, and S. Poddar, Phys. Rev. D **73**, 075014 (2006).
[103] A. Datta and S. Poddar, Phys. Rev. D **75**, 075013 (2007).
[104] A. Datta and S. Poddar, Phys. Rev. D **79**, 075021 (2009).
[105] Z. Marshall, B. A. Ovrut, A. Purves, and S. Spinner, Phys. Lett. B **732**, 325 (2014).
[106] R. Bose, A. Datta, A. Kundu, and S. Poddar, Phys. Rev. D **90**, 035007 (2014).
[107] E. J. Chun, S. Jung, H. M. Lee, and S. C. Park, Phys. Rev. D **90**, 115023 (2014).
[108] A. Choudhury and A. Datta, Mod. Phys. Lett. A **27**, 1250188 (2012).
[109] R. Grober, M. Muhlleitner, E. Popenda, and A. Wlotzka, Eur. Phys. J. C **75**, 420 (2015).
[110] G. Ferretti, R. Franceschini, C. Petersson, and R. Torre, Phys. Rev. Lett. **114**, 201801 (2015).
[111] G. Belanger, D. Ghosh, R. Godbole, and S. Kulkarni, J. High Energy Phys. 09 (2015) 214.
[112] S. Chatrchyan *et al.* (CMS Collaboration), Phys. Rev. Lett. **111**, 221801 (2013).
[113] G. Aad *et al.* (ATLAS Collaboration), Phys. Rev. D **90**, 052008 (2014).
[114] A. Chakraborty, D. K. Ghosh, D. Ghosh, and D. Sengupta, J. High Energy Phys. 10 (2013) 122.
[115] J. Eckel, S. Su, and H. Zhang, J. High Energy Phys. 07 (2015) 075.
[116] A. Chakraborty, D. K. Ghosh, S. Mondal, S. Poddar, and D. Sengupta, Phys. Rev. D **91**, 115018 (2015).
[117] J. S. Kim, K. Rolbiecki, K. Sakurai, and J. Tattersall, J. High Energy Phys. 12 (2014) 010.
[118] H. Abe, J. Kawamura, and Y. Omura, J. High Energy Phys. 08 (2015) 089.
[119] T. Han, S. Su, Y. Wu, B. Zhang, and H. Zhang, Phys. Rev. D **92**, 115009 (2015).
[120] CMS Collaboration, Report No. CMS-PAS-SUS-13-018, 2013.
[121] W. Porod, Comput. Phys. Commun. **153**, 275 (2003).
[122] W. Porod and F. Staub, Comput. Phys. Commun. **183**, 2458 (2012).
[123] W. Porod, F. Staub, and A. Vicente, Eur. Phys. J. C **74**, 2992 (2014).
[124] P. Bechtle, O. Brein, S. Heinemeyer, G. Weiglein, and K. E. Williams, Comput. Phys. Commun. **181**, 138 (2010).
[125] P. Bechtle, O. Brein, S. Heinemeyer, G. Weiglein, and K. E. Williams, Comput. Phys. Commun. **182**, 2605 (2011).
[126] P. Bechtle, O. Brein, S. Heinemeyer, O. Stal, T. Stefaniak, G. Weiglein, and K. Williams, *Proc. Sci.*, CHARGED 2012 (2012) 024 [arXiv:1301.2345].
[127] P. Bechtle, O. Brein, S. Heinemeyer, O. Stal, T. Stefaniak, G. Weiglein, and K. E. Williams, Eur. Phys. J. C **74**, 2693 (2014).
[128] P. Bechtle, S. Heinemeyer, O. Stl, T. Stefaniak, and G. Weiglein, Eur. Phys. J. C **74**, 2711 (2014).
[129] P. Bechtle, S. Heinemeyer, O. Stl, T. Stefaniak, and G. Weiglein, J. High Energy Phys. 11 (2014) 039.
[130] J. Alwall, R. Frederix, S. Frixione, V. Hirschi, F. Maltoni, O. Mattelaer, H.-S. Shao, T. Stelzer, P. Torrielli, and M. Zaro, J. High Energy Phys. 07 (2014) 079.
[131] J. Pumplin, D. R. Stump, J. Huston, H. L. Lai, P. M. Nadolsky, and W. K. Tung, J. High Energy Phys. 07 (2002) 012.
[132] W. Beenakker, M. Kramer, T. Plehn, M. Spira, and P. M. Zerwas, Nucl. Phys. **B515**, 3 (1998).
[133] W. Beenakker, R. Hopker, and M. Spira, arXiv:hep-ph/9611232.
[134] T. Sjostrand, S. Mrenna, and P. Z. Skands, J. High Energy Phys. 05 (2006) 026.
[135] https://twiki.cern.ch/twiki/bin/view/LHCPhysics/TtbarNNLO#Top_quark_pair_cross_sections_at.
[136] J. M. Campbell and R. K. Ellis, Phys. Rev. D **62**, 114012 (2000).
[137] S. Dawson, C. Jackson, L. H. Orr, L. Reina, and D. Wackeroth, Phys. Rev. D **68**, 034022 (2003).
[138] F. Febres Cordero, L. Reina, and D. Wackeroth, Phys. Rev. D **78**, 074014 (2008).
[139] R. Frederix, S. Frixione, V. Hirschi, F. Maltoni, R. Pittau, and P. Torrielli, J. High Energy Phys. 09 (2011) 061.
[140] http://www.hep.phy.cam.ac.uk/ lester/mt2/.
[141] ATLAS Collaboration, Report No. ATLAS-CONF-2015-015, 2015.
[142] D. G. d'Enterria *et al.* (CMS Collaboration), J. Phys. G **34**, 2307 (2007).
[143] W. S. Cho, J. S. Gainer, D. Kim, K. T. Matchev, F. Moortgat, L. Pape, and M. Park, J. High Energy Phys. 05 (2015) 040.
[144] C. Kilic and B. Tweedie, J. High Energy Phys. 04 (2013) 110.
[145] M. L. Graesser and J. Shelton, Phys. Rev. Lett. **111**, 121802 (2013).